On the use of 18Oatm for ice core dating

Extier, Thomas; Landais, Amaelle; Bréant, Camille; Prié, Frédéric; Bazin, Lucie; Dreyfus, Gabrielle; Roche, Didier M.; Leuenberger, Markus

published in
Quaternary Science Reviews
2018

DOI (link to publisher)
10.1016/j.quascirev.2018.02.008

document version
Publisher's PDF, also known as Version of record

Quaternary Science Reviews 185 (2018) 244–257

Contents lists available at ScienceDirect

Quaternary Science Reviews

journal homepage: www.elsevier.com/locate/quascirev

On the use of $\delta^{18}O_{atm}$ for ice core dating

Thomas Extier [a, *], Amaelle Landais [a], Camille Bréant [a], Frédéric Prié [a], Lucie Bazin [a], Gabrielle Dreyfus [b], Didier M. Roche [a, c], Markus Leuenberger [d]

[a] Laboratoire des Sciences du Climat et de l'Environnement, LSCE/IPSL, CEA-CNRS-UVSQ, Université Paris-Saclay, 91191, Gif-sur-Yvette, France
[b] Institute for Governance and Sustainable Development, Washington, DC, 20007, United States
[c] Earth and Climate Cluster, Faculty of Sciences, Vrije Universiteit Amsterdam, Amsterdam, The Netherlands
[d] Climate and Environmental Physics, Physics Institute and Oeschger Center for Climate Research, University of Bern, Sidlerstrasse, 5, 3012, Bern, Switzerland

ARTICLE INFO

Article history:
Received 9 November 2017
Received in revised form
9 February 2018
Accepted 9 February 2018
Available online 27 February 2018

Keywords:
Oxygen isotopes
$\delta^{18}O_{atm}$
Glacial terminations
Water cycle
Ice core
Chronology

ABSTRACT

Deep ice core chronologies have been improved over the past years through the addition of new age constraints. However, dating methods are still associated with large uncertainties for ice cores from the East Antarctic plateau where layer counting is not possible. Indeed, an uncertainty up to 6 ka is associated with AICC2012 chronology of EPICA Dome C (EDC) ice core, which mostly arises from uncertainty on the delay between changes recorded in $\delta^{18}O_{atm}$ and in June 21st insolation variations at 65°N used for ice core orbital dating. Consequently, we need to enhance the knowledge of this delay to improve ice core chronologies.

We present new high-resolution EDC $\delta^{18}O_{atm}$ record (153–374 ka) and $\delta O_2/N_2$ measurements (163–332 ka) performed on well-stored ice to provide continuous records of $\delta^{18}O_{atm}$ and $\delta O_2/N_2$ between 100 and 800 ka. The comparison of $\delta^{18}O_{atm}$ with the $\delta^{18}O_{calcite}$ from East Asian speleothems shows that both signals present similar orbital and millennial variabilities, which may represent shifts in the InterTropical Convergence Zone position, themselves associated with Heinrich events. We thus propose to use the $\delta^{18}O_{calcite}$ as target for $\delta^{18}O_{atm}$ orbital dating. Such a tuning method improves the ice core chronology of the last glacial inception compared to AICC2012 by reconciling NGRIP and mid-latitude climatic records. It is especially marked during Dansgaard-Oeschger 25 where the proposed chronology is 2.2 ka older than AICC2012. This $\delta^{18}O_{atm} - \delta^{18}O_{calcite}$ alignment method applied between 100 and 640 ka improves the EDC ice core chronology, especially over MIS 11, and leads to lower ice age uncertainties compared to AICC2012.

1. Introduction

The EPICA Dome C (EDC) ice core provides a continuous 800 ka (thousands of years before 1950) record of past atmospheric greenhouse gases concentrations (Spahni et al., 2005; Loulergue et al., 2008; Lüthi et al., 2008) and Antarctic surface temperature (Jouzel et al., 2007), contributing to paleoclimatic and paleoenvironmental information. However the uncertainties arising from ice core dating methodologies limit the interpretation of records in terms of past climate dynamics, especially on long time scales. Establishing a causal relationship between orbital forcing (precession or obliquity) and polar temperature over deglaciations, or making the link between polar ice cores and low latitudes climate archives is particularly critical in this context. The EDC3 chronology (Parrenin et al., 2007) has been developed using ice flow modeling, peaks in ^{10}Be record and orbital dating constraints based on air content and $\delta^{18}O_{atm}$ ($\delta^{18}O$ of atmospheric O_2), especially in the deeper part of the ice core (300–800 ka, Dreyfus et al., 2007). The more recent AICC2012 chronology (Bazin et al., 2013; Veres et al., 2013) was built using revised and additional age constraints compared to EDC3, especially through the addition of numerous gas and ice stratigraphic links, combined with the inverse dating method DATICE (Lemieux-Dudon et al., 2010) to provide a coherent chronology for four Antarctic ice cores (EDC, Vostok, EPICA Dronning Maud Land - EDML, TALos Dome ICE core - TALDICE) and one Greenland ice core (NorthGRIP - NGRIP). An uncertainty of up to 6 ka is associated with the AICC2012 EDC chronology for the oldest part (Bazin et al., 2013).

* Corresponding author.
E-mail address: thomas.extier@lsce.ipsl.fr (T. Extier).

https://doi.org/10.1016/j.quascirev.2018.02.008
0277-3791/

Despite the numerous dating constraints implemented in the EDC3 and AICC2012 chronologies, there are evidences that these chronologies should be revised. First, the comparison of Dome F (DFO2006) and AICC2012 age scales over the Marine Isotope Stage (MIS) 5 features an age difference with maximum values of 4.5 and 3.1 ka over MIS 5d and MIS 5b respectively (Fujita et al., 2015). Second, the comparison of the NGRIP $\delta^{18}O_{ice}$ record on the AICC2012 chronology with lower latitudes records such as the Northern rim of the Alps speleothems - NALPS (Boch et al., 2011) highlights inconsistencies of several millennia between chronologies over the last glacial inception (Veres et al., 2013).

Total air content has largely been used for the establishment of EDC chronologies (Parrenin et al., 2007) based on its link with the integrated local summer insolation (Raynaud et al., 2007). Another ice core parameter, the $\delta O_2/N_2$, was proposed as an orbital tuning tool (Bender, 2002). Indeed, the $\delta O_2/N_2$ outlines variations at orbital scale that are in phase with the local summer insolation (Bender, 2002; Kawamura et al., 2007; Suwa and Bender, 2008; Landais et al., 2012; Bazin et al., 2016). The relationship between $\delta O_2/N_2$ and the local summer insolation is likely established through the near-surface snow metamorphism (Hutterli et al., 2010) that influences snow density down to the pore close-off depth during firnification (Fujita et al., 2009). Then, at close-off, trapping process favors the loss of O_2 compared to N_2 molecules (Battle et al., 1996; Huber et al., 2006; Severinghaus and Battle, 2006). This link can be used to build ice core chronologies when associated with an appropriate error bar.

The $\delta^{18}O_{atm}$ measured in ice cores is a complex signal that can still be related to the low latitude water cycle (Landais et al., 2010; Seltzer et al., 2017). This marker combines variations in biospheric and low latitude water cycle processes, thus integrating changes in global sea level, water cycle and biosphere productivity through photosynthesis and respiration fluxes (Bender et al., 1994). Although the drivers of $\delta^{18}O_{atm}$ variations over the last 800 ka remain poorly known, several studies have highlighted the resemblance between those variations and the precession signal or mid-June 65°N insolation (Jouzel et al., 1996; Petit et al., 1999; Dreyfus et al., 2007; Landais et al., 2010). A 5–6 ka lag is classically applied between precession and $\delta^{18}O_{atm}$ minima, as primarily observed over Termination I (Bender et al., 1994; Jouzel et al., 1996, 2002; Petit et al., 1999; Dreyfus et al., 2007). The existence of this lag and the difficulty to explain it due to the complexity of the $\delta^{18}O_{atm}$ signal are the main reasons why EDC ice core chronologies are associated with a 6 ka uncertainty. A reduction of this error bar would allow the use of $\delta^{18}O_{atm}$ as a better dating tool.

Advances in the use of $\delta^{18}O_{atm}$ for chronology construction goes through a better understanding of processes affecting the $\delta^{18}O_{atm}$. It has been suggested that precessional variations in solar input can play a key role in influencing the low latitude water cycle and hence $\delta^{18}O_{atm}$ through changes of the ITCZ (InterTropical Convergence Zone) position (Bender et al., 1994; Landais et al., 2010). The role of precession or northern summer insolation on ITCZ shifts is expected from interhemispheric atmospheric energy balance (Cheng et al., 2016). It is visible in East Asian $\delta^{18}O_{calcite}$ record with the additional imprint of millennial scale variability. The resemblance between $\delta^{18}O_{atm}$ and East Asian $\delta^{18}O_{calcite}$ has already been highlighted (Wang et al., 2008; Severinghaus et al., 2009; Landais et al., 2010). A recent speleothem composite $\delta^{18}O_{calcite}$ record from Chinese caves supports the idea that the last seven glacial terminations recorded in $\delta^{18}O_{calcite}$ were driven by Northern Hemisphere summer insolation changes (Cheng et al., 2016). Since speleothem records are precisely dated, this composite record is a good candidate to progress in our use of $\delta^{18}O_{atm}$ as a dating constraint.

In this paper we first present new high-resolution $\delta^{18}O_{atm}$ and $\delta O_2/N_2$ reference records from EDC ice core over the last 400 ka and hence complement the study of Bazin et al. (2016) focused on the 300–800 ka period. We use these composite records to decipher the orbital and millennial components of the $\delta^{18}O_{atm}$ signal and explore mechanisms driving the $\delta^{18}O_{atm}$ variations in comparison with East Asian $\delta^{18}O_{calcite}$. We thus propose a novel method using the $\delta^{18}O_{atm}$ data to improve the ice core dating and find support for it through an application over the last 640 ka.

2. Methods

2.1. Analytical method

All analyzed samples come from the EPICA Dome C deep ice core from Antarctica. 75 samples were stored at −50 °C and could be used for both $\delta^{18}O_{atm}$ and $\delta O_2/N_2$ measurements. Additional 333 samples, stored at −20 °C, completed the $\delta^{18}O_{atm}$ series. Except for the 56 samples measured at Princeton University by Dreyfus (2008) for $\delta^{18}O_{atm}$, following the analytical method given in Dreyfus et al. (2010), most of the $\delta^{18}O_{atm}$ and all $\delta O_2/N_2$ analyses have been performed at LSCE using a semi-automatic extraction line (Capron et al., 2010). Before measurement, 3–5 mm of ice are removed from each sample face in order to prevent contamination from exchanges with ambient air. Each day, three ice samples with duplicates are placed in cold flasks and the air in the flask is evacuated. The samples are then melted and left at room temperature for at least 1h30 in order to extract the air trapped in ice samples. The air samples are transferred through water vapor and CO_2 traps one by one and are cryogenically trapped into a manifold immersed in liquid helium (Capron et al., 2010; Bazin et al., 2016). Two exterior air samples are analyzed for each daily batch of measurements. These exterior air samples serve as standard for $\delta O_2/N_2$, $\delta^{18}O_{atm}$ and atmospheric $\delta^{15}N$ measurements, and are used to check the evolution of our internal laboratory standard and the proper functioning of our analytical set-up.

The measurements of the isotopic composition of air extracted from the ice are then performed using a dual inlet Delta V plus (Thermo Electron Corporation) mass spectrometer. A run is composed of 16 measurements for each sample and allows measurements of the composition of $\delta^{18}O$, $\delta^{15}N$, $\delta O_2/N_2$ and CO_2 (mass 44) simultaneously.

2.2. Corrections

The raw data are corrected for several processes such as pressure imbalance and mass interferences following procedures described in Landais et al. (2003a) and Severinghaus et al. (2003). They also need to be calibrated against the mean exterior air values in order to express the $\delta^{18}O_{atm}$, $\delta^{15}N$ and $\delta O_2/N_2$ with respect to the composition of atmospheric air, i.e. the standard of reference for these isotopic and elemental ratios. As we did not observe any evolution in the isotopic measurements of atmospheric air through the period of measurements, the correction with respect to atmospheric air was done using a constant value for each period of measurements. In addition to these standard corrections, we also account for firn fractionation and gas loss effects.

2.2.1. Firn fractionation correction due to diffusive processes

The $\delta^{18}O$ of O_2 and $\delta O_2/N_2$ records must be corrected for processes in the firn diffusive column that directly affect the distribution of isotopes. The associated fractionations are driven either by the Earth's gravity field or by the temperature gradient within the firn column (Severinghaus et al., 1998). In our case, the thermal fractionation correction in East Antarctica is neglected because temperature changes are too slow to create large transient temperature gradients, which lead to the migration of the heavier

species toward the colder regions of the firn column (Goujon et al., 2003; Bréant et al., 2017).

The fractionation induced by the Earth's gravity field is proportional to the mass difference between the considered isotopes: 2 g/mol for $^{18}O/^{16}O$ ratio, 1 g/mol for the $^{15}N/^{14}N$ ratio and 4 g/mol for the O_2/N_2 ratio (Craig et al., 1988; Schwander, 1989; Severinghaus et al., 1998). Hence, the $\delta^{18}O$ will be affected twice as much as the $\delta^{15}N$ by the gravitational signal. To correct the $\delta^{18}O_{atm}$ from gravitational fractionation effects, we use the measurements of $\delta^{15}N$ of N_2 performed on the same samples using Eq. (1), assuming that $\delta^{15}N$ enrichment in air bubbles is only of gravitational origin. The $\delta O_2/N_2$ is also corrected using $\delta^{15}N$ of N_2 but with a factor 4 in Eq. (2).

$$\delta^{18}O_{atm\,corrected} = \delta^{18}O_{atm} - 2 \times \delta^{15}N \quad (1)$$

$$\delta O_2/N_{2corrected} = \delta O_2/N_2 - 4 \times \delta^{15}N \quad (2)$$

2.2.2. Gas loss correction

Several authors have shown that gas loss fractionation affects the $\delta^{18}O$ of O_2 when ice is stored for a long time above -50 °C (Landais et al., 2003b; Dreyfus et al., 2007; Kawamura et al., 2007; Suwa and Bender, 2008; Severinghaus et al., 2009). This loss of O_2 affects the $\delta^{18}O_{atm}$ following a linear relationship (Landais et al., 2003b, Appendix A) and has to be taken into account:

$$\delta^{18}O_{atm\,corrected} = \delta^{18}O_{atm} + (\delta O_2/N_2 + 10) \times 0.01 \quad (3)$$

The resulting pooled standard deviation is 0.03‰ for the $\delta^{18}O_{atm}$ measurements and 0.37‰ for the $\delta O_2/N_2$ measurements after taking all corrections into account.

2.3. New records

We present here new $\delta^{18}O_{atm}$ measurements on 408 samples regrouping different data sets from LSCE and Princeton University (Table 1). We also present 75 new $\delta O_2/N_2$ measurements performed on EDC ice samples stored at -50 °C until their analysis (Table 1). The common AICC2012 chronology (Bazin et al., 2013; Veres et al., 2013) was used to convert the sample depths into corresponding gas and ice ages.

3. Results

3.1. $\delta^{18}O_{atm}$ over the last 800 ka

Our dataset complements previously available EDC $\delta^{18}O_{atm}$ series between 0 and 40 ka, 98–152 ka and 300–800 ka (Dreyfus et al., 2007, 2008; Landais et al., 2013; Bazin et al., 2016) with an overlap between 300 and 374 ka. To display a continuous $\delta^{18}O_{atm}$ record over the last 800 ka, the $\delta^{18}O_{atm}$ record presented on Fig. 1 between 40 and 98 ka has been obtained from the Vostok ice core (Petit et al., 1999). The common EDC $\delta^{18}O_{atm}$ section between 300 and 374 ka shows a good agreement between the previous and new data with comparable trends and amplitude variations. Thanks to this new record, the $\delta^{18}O_{atm}$ over the last four terminations is recorded at high temporal resolution (~300 years for Terminations I and II, ~160 years for Termination III and ~700 years for Termination IV, Fig. 1), the highest resolution corresponding to Termination III.

Fig. 1 displays the good correlation between the EDC $\delta^{18}O_{atm}$ signal and June 21st insolation variations at 65°N as already observed in previous studies (Petit et al., 1999; Dreyfus et al., 2007). The amplitudes of $\delta^{18}O_{atm}$ variations and June 21st insolation at 65°N are comparable, except for two distinct periods: 190–230 ka and around 430 ka. The high-resolution EDC record permits to look in details at the behavior of $\delta^{18}O_{atm}$ during terminations. Terminations I, II, IV and V display a large amplitude $\delta^{18}O_{atm}$ decrease in parallel with relatively large variations in June 21st insolation at 65°N and important increases in sea-level and δD of EDC ice core (Fig. 1). On the opposite, the $\delta^{18}O_{atm}$ record over Termination III is associated with a lower amplitude for the decrease and displays a superimposed millennial-scale variability (inset of Fig. 1) as previously identified for the last glacial period by Landais et al. (2007) and Severinghaus et al. (2009). The reason why Termination III exhibits a different signal compared to Terminations I, II, IV and V, may be linked to the fact that these four terminations are associated with strong Heinrich events identified by high IRD imprint (Ice Rafted Debris, characterized by large amount of detrital quartz in the sediments), while Termination III is associated with a series of Heinrich events of smaller IRD imprint as well as a smaller sea level change (Fig. 1).

The long EDC $\delta^{18}O_{atm}$ record can readily be compared to the Vostok and Dome F data over the last 400 ka (Petit et al., 1999; Kawamura et al., 2007, Fig. 2). While Vostok and Dome C are both drawn on the AICC2012 chronology, the Dome F chronology DFO2006 has been transferred to AICC2012 by Bazin et al. (2016) using the volcanic synchronization of EDC and Dome F over the last 216 ka (Fujita et al., 2015). The resolution of Vostok and Dome F records is lower than the EDC record (~1.27 ka and ~1.15 ka compared to ~0.55 ka resolution respectively for the last 400 ka). This difference in resolution is especially large during terminations. The orbital trend is similar for the three $\delta^{18}O_{atm}$ signals, with a clear resemblance with the 65°N mid-June insolation. The amplitudes of the $\delta^{18}O_{atm}$ signals are also identical except when the higher resolution of the EDC record allows a better description of $\delta^{18}O_{atm}$ peaks (e.g. between 240 and 280 ka, Fig. 2).

3.2. $\delta O_2/N_2$ record

$\delta O_2/N_2$ data measured on EDC ice stored at −50 °C have already been published between 338 and 800 ka and also between 100 and 161 ka (Landais et al., 2012; Bazin et al., 2016). We present here new measurements for the time period covering 163–332 ka (Fig. 3). These new data allow a continuous record from 100 to 800 ka on EDC well-conserved ice. The most recent 100 ka do not show clear insolation imprinted variability due to large $\delta O_2/N_2$ depletions at the air bubbles/clathrates transition (Bender, 2002).

On Fig. 3, we can see clear similarities between the local December 21st insolation (75°S for EDC) and $\delta O_2/N_2$ variations as evidenced in previous studies (Bender, 2002; Kawamura et al.,

Table 1
Summary of the new EDC $\delta^{18}O_{atm}$ and $\delta O_2/N_2$ data.

Year	Measurements	Laboratory	Number of samples	Depth (m)	Age (ka)
2014 to 2017	$\delta^{18}O_{atm}$	LSCE	352	1872.23–2664.72	153.03–374.22
2008	$\delta^{18}O_{atm}$	Princeton University (Dreyfus, PhD thesis)	56	2261.63–2351.88	235.01–256.35
2014 to 2016	$\delta O_2/N_2$	LSCE	75	1904.07–2561.87	163.56–332.03

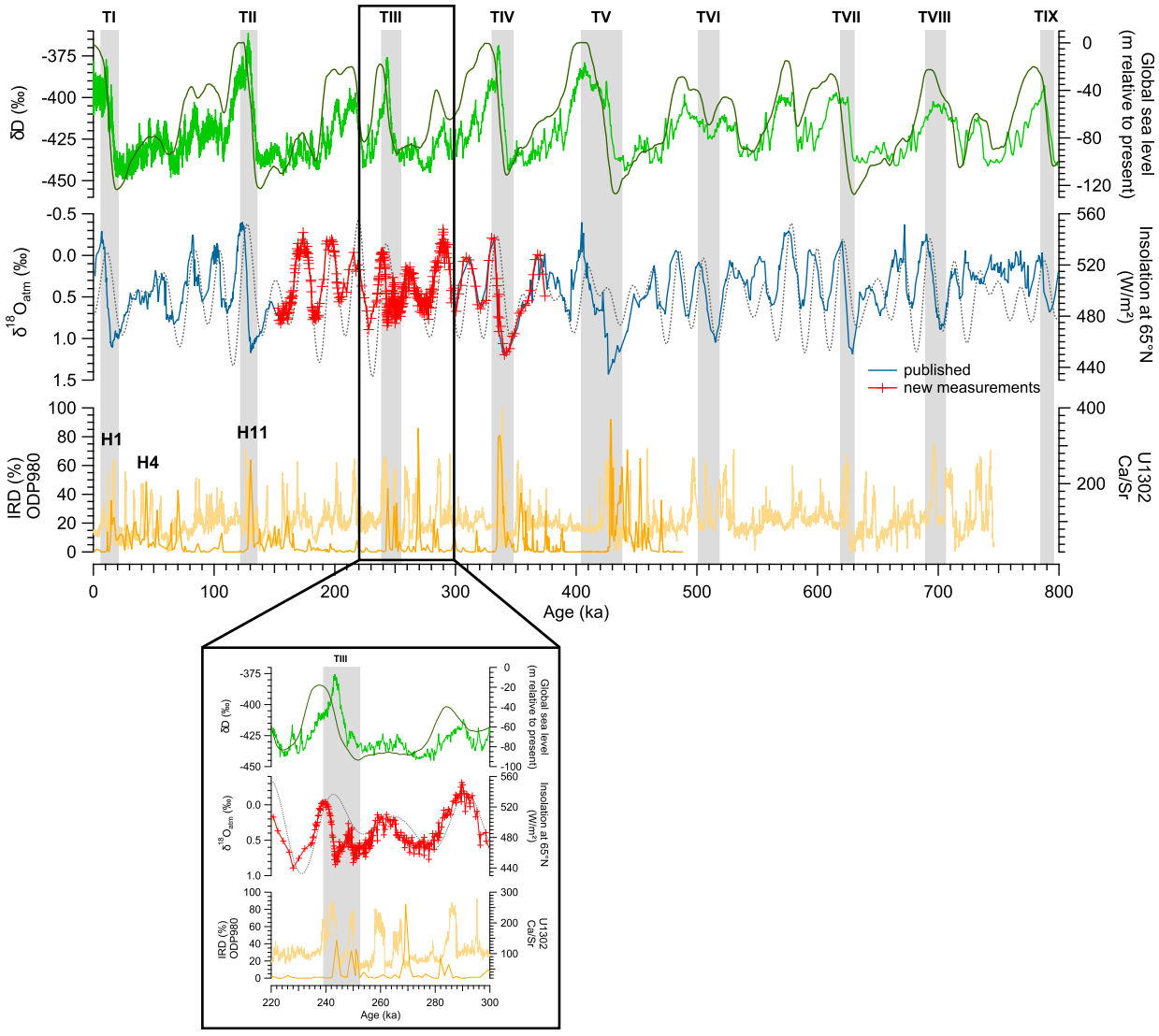

Fig. 1. Top: Record over the last 800 ka of ice δD from EDC (light green: Jouzel et al., 2007) and global sea level estimate (green: Bintanja et al., 2005). Middle: Composite EDC-Vostok $\delta^{18}O_{atm}$ variations (blue: Petit et al., 1999; Dreyfus et al., 2007, 2008; Landais et al., 2013; Bazin et al., 2016, red: this study) on the AICC2012 chronology (Bazin et al., 2013; Veres et al., 2013) and the June 21st insolation signal at 65°N (grey: Laskar et al., 2004). Bottom: The percentage of IRD at site ODP980 (orange: McManus et al., 1999) transferred on AICC2012 timescale (Vazquez Riveiros, Comm. Pers.) and the Ca/Sr ratio at site U1302, a proxy of Laurentide sourced IRD (light orange: Channell et al., 2012). The grey bars highlight the glacial terminations. The inset shows a focus on the high-resolution data over Termination III. (For interpretation of the references to colour in this figure legend, the reader is referred to the Web version of this article.)

2007). Even if there is a clear correspondence between $\delta O_2/N_2$ and local summer insolation variations, the relative amplitudes of the two signals do not match, as already observed for the period 350–800 ka (Bazin et al., 2016).

Landais et al. (2012) and Bazin et al. (2016) identified a general decreasing $\delta O_2/N_2$ trend over the last 800 ka by 7.9‰ (1σ) per million years (Ma). Stolper et al. (2016) have interpreted the mean decrease of 8.4‰ per million years (±0.2‰ per million years, 1σ) for all $\delta O_2/N_2$ record (EDC, Vostok and Dome F) as a result of the changes in organic carbon fluxes over the last 800 ka. Still, many of the $\delta O_2/N_2$ data presented in the cited work were affected by gas loss, hence questioning the robustness of this long $\delta O_2/N_2$ trend. Our new measurements, free from gas loss correction, show that this long-term trend is significant and we obtain a new value of 7.0 ± 0.6‰ per million years (1σ) decrease of $\delta O_2/N_2$ for the whole EDC curve (Fig. 4).

The EDC $\delta O_2/N_2$ record can also be compared with Vostok (Suwa and Bender, 2008) and Dome F (Kawamura et al., 2007) measurements covering the last 400 ka (Fig. 4). Note that the EDC record is the only one that is not much affected by gas loss. Dome F and Vostok $\delta O_2/N_2$ data displayed on Fig. 4 were obtained on samples stored at −20 °C and corrected for gas loss. However, similar decreasing trends are observed for all three sites with a higher value for EDC than for Dome F and Vostok (Fig. 4). The variations at orbital scale are also observed on these three records between 100 and 150 ka, as previously noted by Bazin et al., (2016). Furthermore, the Vostok curve shows lower values and higher amplitude than the other two sites, most probably due to the gas loss influence.

4. Discussion

4.1. $\delta^{18}O_{atm}$ orbital variations

Orbital tuning is largely used for dating paleoclimate archives. Still, one of the main difficulties is to properly determine the orbital

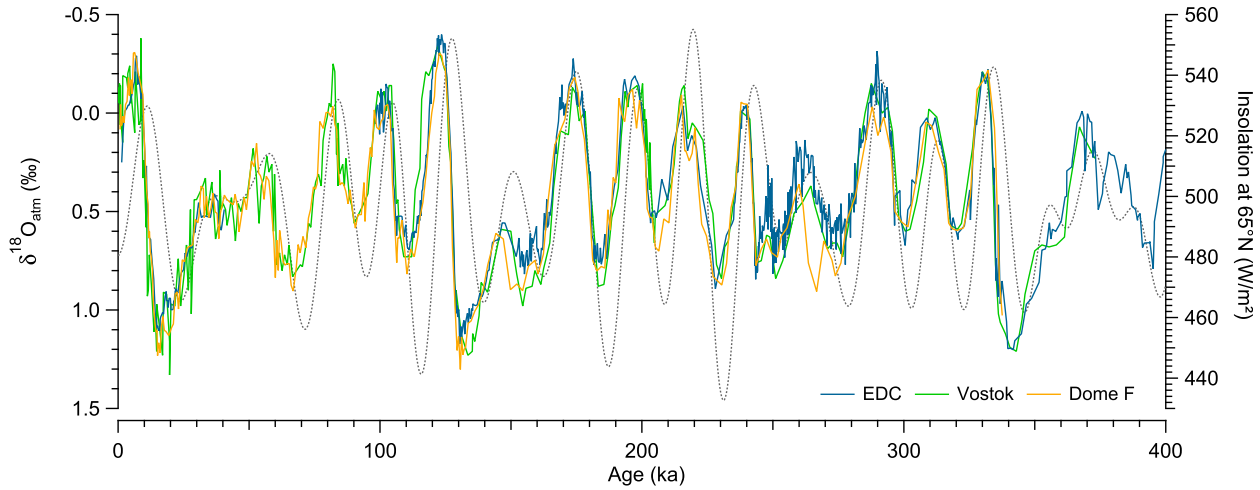

Fig. 2. Comparison of EDC $\delta^{18}O_{atm}$ data (blue: Dreyfus et al., 2007, 2008; Landais et al., 2013; Bazin et al., 2016; this study), Vostok record (green: Petit et al., 1999; Bazin et al., 2013) and Dome F record (orange: Kawamura et al., 2007). Dome C and Vostok are drawn on the AICC2012 chronology. Dome F is presented on AICC2012 between 0 and 216 ka using volcanic synchronization (Fujita et al., 2015). The June 21st insolation at 65°N is also represented (grey: Laskar et al., 2004). (For interpretation of the references to colour in this figure legend, the reader is referred to the Web version of this article.)

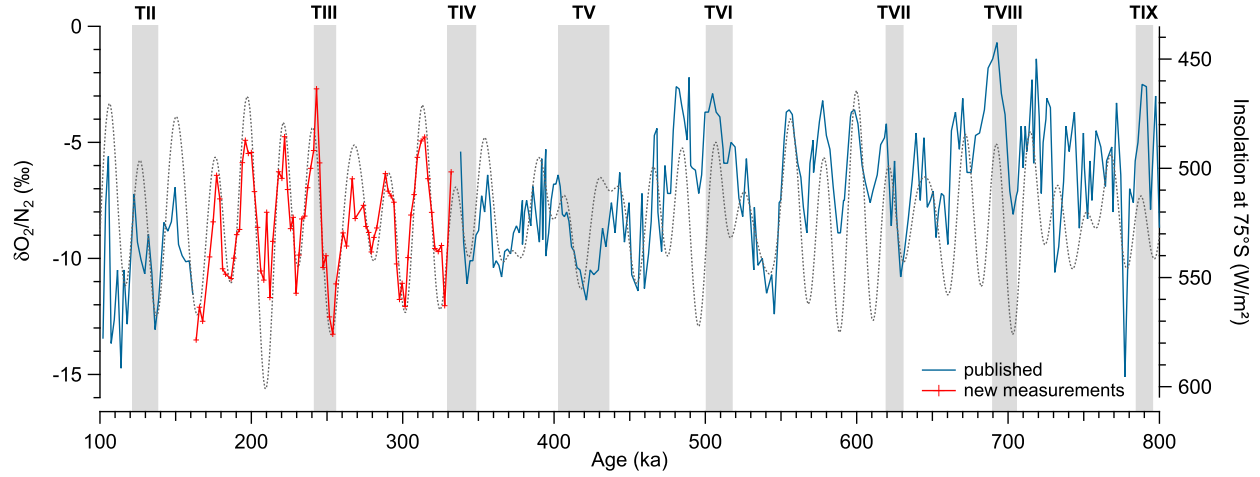

Fig. 3. EDC records of $\delta O_2/N_2$ (blue: Landais et al., 2012; Bazin et al., 2016, red: this study) on the AICC2012 chronology superimposed to the 75°S summer solstice (December 21st) insolation (grey: Laskar et al., 2004). The grey bars highlight the glacial terminations. (For interpretation of the references to colour in this figure legend, the reader is referred to the Web version of this article.)

target. This is particularly important for $\delta^{18}O_{atm}$ because of the multiplicity of mechanisms involved in driving its variations. Some studies used the June 21st insolation at 65°N as target for $\delta^{18}O_{atm}$ (Jouzel et al., 1996; Shackleton, 2000; Dreyfus et al., 2007), or even the 20°N summer insolation (Bender et al., 1994; Malaizé et al., 1999). In parallel, $\delta^{18}O_{calcite}$ from East Asian speleothems, also largely linked to water cycle dynamic on a large regional scale (Caley et al., 2014) aligns well with the boreal summer insolation, July 21st at 65°N (or integrated summer insolation over June-July-August; Wang et al., 2001, 2008).

Some phase delays have been observed between orbital variations of proxy records and their chosen target. On average, there is a ~3 ka lead of precession (2 ka lead of July 21st insolation) over East Asian $\delta^{18}O_{calcite}$ variations through the last climatic cycles (Wang et al., 2008; Clemens et al., 2010). This is 2 ka larger than the mean delay obtained over the last climatic cycle between modeled $\delta^{18}O_{calcite}$ variations of East Asian speleothems and precession using an intermediate complexity fully coupled climate model forced only by orbital parameters, ice sheet size and greenhouse gases concentration (i.e. no freshwater forcing representing the influence of Heinrich events, Caley et al., 2014). The 2 ka additional lag between $\delta^{18}O_{calcite}$ variations of East Asian speleothems and summer insolation may thus be attributed to the influence of Heinrich events on low latitude water cycle through shifts of the ITCZ. Ice core $\delta^{18}O_{atm}$ variations also exhibit a lag with respect to its orbital target: a lag of 5–6 ka has been observed between the June 21st insolation and $\delta^{18}O_{atm}$ variations over the last two deglaciations (Dreyfus et al., 2007; Bazin et al., 2016). The influence of Heinrich events on this lag can also be questioned. Based on the similarity between $\delta^{18}O_{atm}$ and speleothems, already noted by Wang et al. (2008), Severinghaus et al. (2009) and Landais et al. (2010), we choose the July 21st insolation at 65°N as target for the $\delta^{18}O_{atm}$ in the following.

The simplest way to look at the delay between the $\delta^{18}O_{atm}$ and the July 21st insolation is to draw the temporal evolution of the shift between $\delta^{18}O_{atm}$ and its orbital target over time. This is however circular since the ice core chronology, before annual layer counting (60 ka), is partly deduced from $\delta^{18}O_{atm}$ tuning with the June 21st

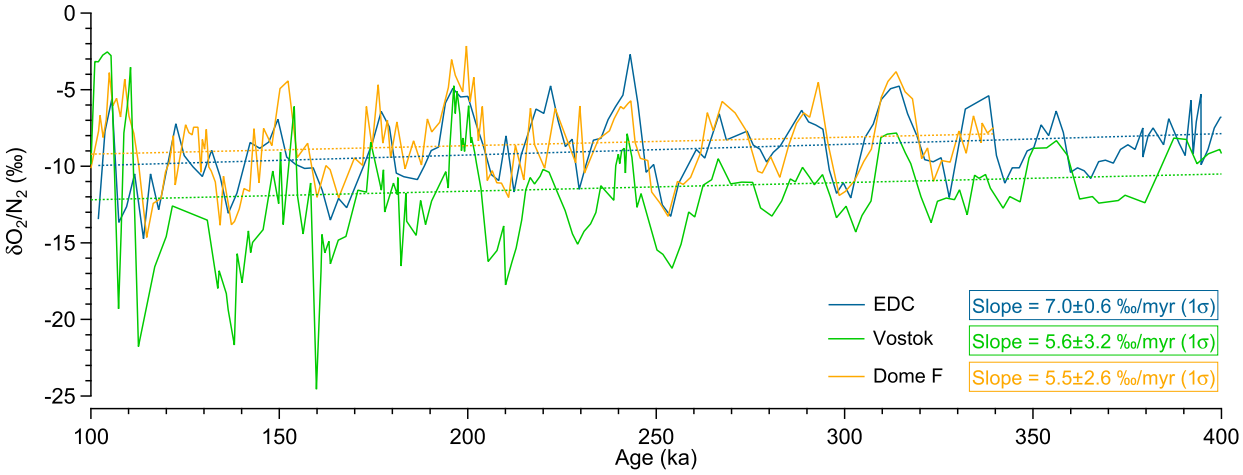

Fig. 4. Inter-comparison of $\delta O_2/N_2$ records from EDC (blue: Landais et al., 2012; Bazin et al., 2016; this study), Vostok (green: Suwa and Bender, 2008) and Dome F (orange: Kawamura et al., 2007) presented on the AICC2012 chronology. The Dome F data are transferred on the AICC2012 chronology using the volcanic matching of Fujita et al. (2015) over the period 0–216 ka. (For interpretation of the references to colour in this figure legend, the reader is referred to the Web version of this article.)

insolation accounting for a 6 ka delay (Dreyfus et al., 2007; Parrenin et al., 2007; Bazin et al., 2013). To keep a critical eye on this assumption, we look in parallel at the delay between the $\delta O_2/N_2$ variations and its orbital target, the local summer solstice insolation, as already proposed by Bazin et al. (2016). The idea behind this comparison is the following: if a large delay is observed synchronously between $\delta O_2/N_2$ vs local summer solstice insolation and between $\delta^{18}O_{atm}$ vs June 21st insolation at 65°N, this delay is due to an issue with the chronology. If the delay is observed only for one of the two comparisons, it questions the phasing between the proxy variation and its orbital target.

The delay is estimated through the use of Match protocol (Lisiecki and Lisiecki, 2002). This method uses dynamic programming with penalty functions to constrain accumulation rates in order to find a realistic and optimal fit between two records. Before matching $\delta^{18}O_{atm}$ and $\delta O_2/N_2$ to their respective orbital targets (July 21st insolation at 65°N and December 21st insolation at 75°S), the data have been normalized by subtracting the mean from each series and then dividing by the series' standard deviation. Using the normalized data it is then possible to calculate the age differences between the original series and the tuned series to explore the delay between each proxy series and their orbital targets (Fig. 5).

The difference between (1) the delay $\delta^{18}O_{atm}$ vs July 21st insolation at 65°N and (2) the delay $\delta O_2/N_2$ vs December 21st insolation at 75°S provides a mean of discerning between lags resulting from chronological tuning and climate mechanisms (Fig. 5). Still, because of scatter in the $\delta O_2/N_2$ data, this curve may be associated with some uncertainties such as between 100 and 110 ka. Furthermore, the low correlation between $\delta O_2/N_2$ and its orbital target before 650 ka limits the interpretation of the delay over this period. Making the assumption that $\delta O_2/N_2$ is tied to its orbital target without delay (Kawamura et al., 2007), we propose that the most prominent peaks in the black curve reflect the largest delays between the July 21st insolation at 65°N and the $\delta^{18}O_{atm}$ variations. We highlight periods where insolation is in advance by more than 5 ka compared to the $\delta^{18}O_{atm}$ signal at 135, 250, 340, 405 and 430 ka (Fig. 5). In addition, periods where $\delta^{18}O_{atm}$ is in advance with respect to insolation are highlighted at 376 and 445 ka. Most of the identified peaks (at 135, 250, 340 and 430 ka) correspond to the occurrence of large or repeated Heinrich events (Fig. 5) including those associated with Terminations II, III, IV and V (no $\delta O_2/N_2$ are available for Termination I because of poor ice core quality). The two remaining peaks (at 376 and 445 ka) are associated with poor resemblance between the $\delta O_2/N_2$ or $\delta^{18}O_{atm}$ and their orbital targets and should thus be considered with caution. For the remaining periods, the delay between $\delta^{18}O_{atm}$ and the July 21st insolation at 65°N corrected from the delay between $\delta O_2/N_2$ and its insolation target is always lower than 5 ka, hence suggesting that the systematic shift of 5 ka (or 6 ka) between $\delta^{18}O_{atm}$ and July 21st insolation at 65°N (or the June 21st insolation at 65°N) is not optimal for ice core chronology construction.

4.2. Drivers of the millennial variations

Heinrich events and the millennial climate variability of the last glacial period have already been shown to leave an imprint on the $\delta^{18}O_{atm}$ signal through the influence of the low latitude hydrological cycle (Landais et al., 2007, 2010; Severinghaus et al., 2009; Reutenauer et al., 2015; Seltzer et al., 2017). Indeed, southward ITCZ shifts during Heinrich events are associated with changes in the biosphere productivity and in the isotopic composition, leading to increases in $\delta^{18}O_{atm}$ (Reutenauer et al., 2015).

Due to the long residence time of oxygen in the atmosphere (1–2 ka), the signature of millennial events on the $\delta^{18}O_{atm}$ record is smoothed. Severinghaus et al. (2009) proposed to look at the drivers of $\delta^{18}O_{atm}$ changes, themselves being expected to bear a millennial-scale signature. They thus introduce the empirical parameter, $\Delta\varepsilon_{LAND}$ as defined in Eq. (4), representing the changes in water cycle $\delta^{18}O$ and fractionation during oxygen uptake driving the relative changes of $\delta^{18}O_{atm}$ with respect to global $\delta^{18}O_{sea\ water}$ (hence Dole effect).

$$\Delta\varepsilon_{LAND} = \left[\tau \times \frac{d\delta^{18}O_{atm}}{dt} + \delta^{18}O_{atm} - \delta^{18}O_{sea\ water}\right] \times \frac{1}{f_L} \quad (4)$$

τ is the residence time of oxygen in the atmosphere (1 ka), $d\delta^{18}O_{atm}/dt$ is the temporal derivative of $\delta^{18}O_{atm}$, $\delta^{18}O_{sea\ water}$ is the global isotopic composition of sea water, whose evolution over the last climatic cycles can be obtained from Lisiecki and Raymo (2005), and f_L is the fraction of oxygen photosynthesis occurring on land (considered constant through time and equal to 0.65 based on the discussion in Blunier et al., 2002). $\Delta\varepsilon_{LAND}$ has been calculated based on new high resolution $\delta^{18}O_{atm}$ record (Appendix B) and is displayed on Fig. 6. As observed for the Siple and WAIS ice cores (Seltzer et al., 2017), the $\Delta\varepsilon_{LAND}$ deduced from the $\delta^{18}O_{atm}$ data from Dome C (and Vostok between 41 and 98 ka) displays strong

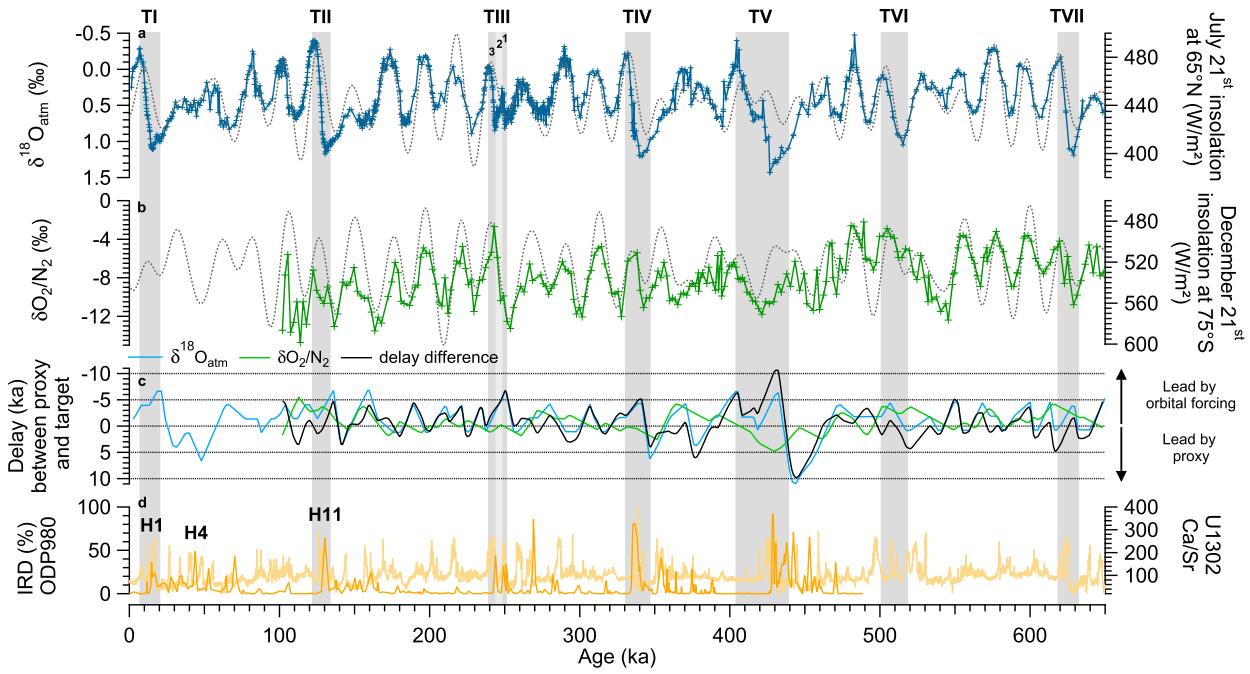

Fig. 5. Evolution of the time delay over the last 650 ka. a: $\delta^{18}O_{atm}$ record (blue: Petit et al., 1999; Dreyfus et al., 2007, 2008; Landais et al., 2013; Bazin et al., 2016; this study) and its orbital forcing (grey: July 21st insolation at 65°N, Laskar et al., 2004). b: $\delta O_2/N_2$ record (green: Landais et al., 2012; Bazin et al., 2016; this study) associated with its orbital forcing (grey: December 21st insolation at 75°S, Laskar et al., 2004). The delay between the original data ($\delta^{18}O_{atm}$ and $\delta O_2/N_2$) and the results after optimal alignment with their respective orbital targets using Match Protocol are shown next. c: The light blue curve represents the age difference between the original $\delta^{18}O_{atm}$ record and the tuned $\delta^{18}O_{atm}$ signal on the July 21st insolation at 65°N and the light green curve represents the age difference between the original $\delta O_2/N_2$ record and the tuned $\delta O_2/N_2$ signal on the December 21st insolation at 75°S. The black curve is the difference between the light blue curve and the light green curve, hence the delay of $\delta^{18}O_{atm}$ vs its insolation target assuming that $\delta O_2/N_2$ should always be in phase with local summer solstice insolation (Bender, 2002; Kawamura et al., 2007). The EDC data are presented on the AICC2012 chronology. d: The percentage of IRD at site ODP980 (orange: McManus et al., 1999) transferred on AICC2012 timescale (Vazquez Riveiros, Comm. Pers.) as well as the Ca/Sr ratio at site U1302, a proxy of Laurentide sourced IRD are also displayed (light orange: Channell et al., 2012). (For interpretation of the references to colour in this figure legend, the reader is referred to the Web version of this article.)

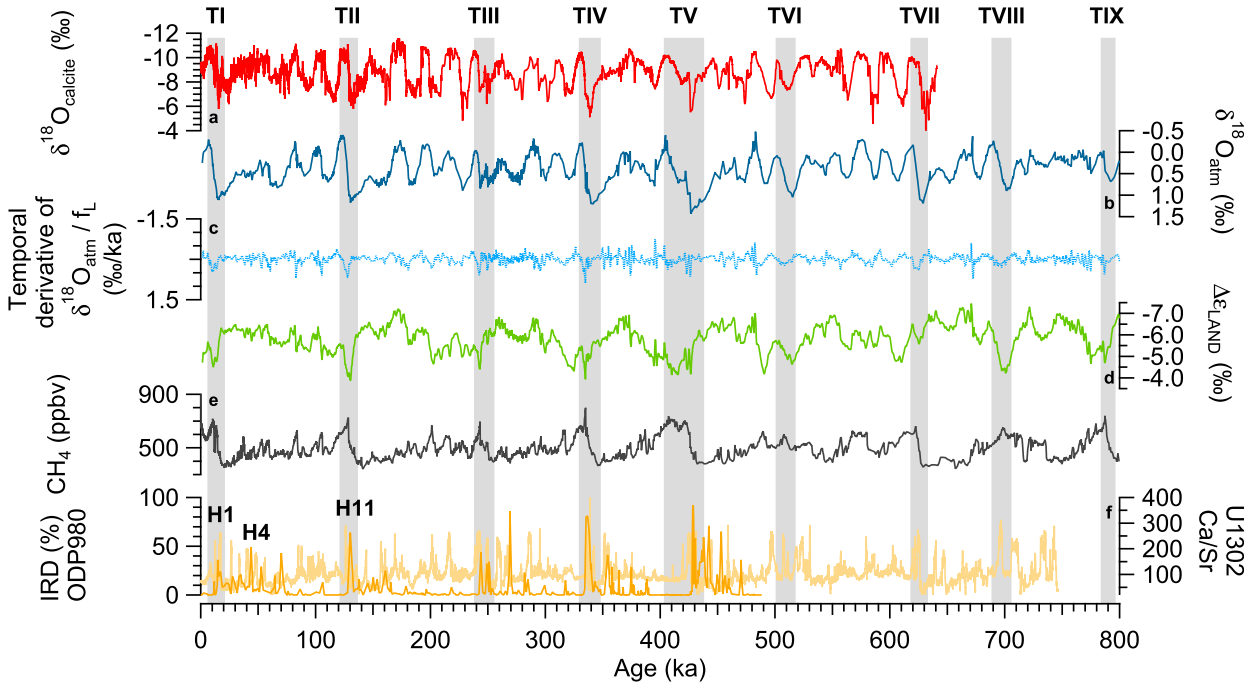

Fig. 6. a: $\delta^{18}O_{calcite}$ composite record from Chinese caves (Cheng et al., 2016). b: $\delta^{18}O_{atm}$ record (Petit et al., 1999; Dreyfus et al., 2007, 2008; Landais et al., 2013; Bazin et al., 2016; this study). c: The temporal derivative of the $\delta^{18}O_{atm}$ divided by the fraction of oxygen photosynthesis occurring on land f_L. d: The inferred change in terrestrial $^{18}O/^{16}O$ fractionation $\Delta\varepsilon_{LAND}$ (based on Severinghaus et al., 2009). e: CH_4 concentration measured on EDC ice core (Loulergue et al., 2008). f: The percentage of IRD at site ODP980 (orange: McManus et al., 1999) transferred on AICC2012 timescale (Vazquez Riveiros, Comm. Pers.) and the Ca/Sr ratio at site U1302 used for Heinrich events identification (light orange: Channell et al., 2012). The $\delta^{18}O_{atm}$, $\Delta\varepsilon_{LAND}$, CH_4 and the percentage of IRD are presented on the AICC2012 chronology. (For interpretation of the references to colour in this figure legend, the reader is referred to the Web version of this article.)

increases corresponding to Heinrich event 1. Deeper in time, $\Delta\varepsilon_{LAND}$ also strongly increases during Terminations II, III, IV, V, VI, VIII and IX (Fig. 6). Such increases are partly driven by the Dole effect term $\delta^{18}O_{atm}$ - $\delta^{18}O_{sea\ water}$ in Eq. (4) through delays of several millennia between the decreases in $\delta^{18}O_{sea\ water}$ and $\delta^{18}O_{atm}$ during terminations.

In addition to the $\delta^{18}O_{sea\ water}$ component, $\Delta\varepsilon_{LAND}$ as driver of $\delta^{18}O_{atm}$ on land is expected to be linked to the low latitude water cycle on land, and, hence to be associated with southward shift of the ITCZ, expressed as Weak Monsoon Intervals (WMI) in East Asia. This influence is also responsible for part of the positive $\Delta\varepsilon_{LAND}$ excursions during terminations associated with Heinrich events through the temporal derivative term $d\delta^{18}O_{atm}/dt$. A link between $\Delta\varepsilon_{LAND}$, East Asian $\delta^{18}O_{calcite}$ and CH_4 is expected over the last 800 ka through common influences of southward shift of the ITCZ, as already observed over the last glacial period (Severinghaus et al., 2009; Seltzer et al., 2017). The comparison between $\Delta\varepsilon_{LAND}$ and $\delta^{18}O_{calcite}$ records is however not obvious when looking at long time periods (i.e. several glacial-interglacial cycles, Fig. 6). Overall, the global correspondence is much better when comparing $\delta^{18}O_{atm}$ to $\delta^{18}O_{calcite}$ with maximum correlation over the last 224 ka ($R^2 = 0.81$, Landais et al., 2010) and a maximum R^2 of 0.70 over the last 640 ka (this study). Moreover, the temporal derivative term does not match well with $\delta^{18}O_{calcite}$ over the full 640 ka record (Fig. 6) while there is a clear resemblance over the last glacial period (Severinghaus et al., 2009). Similarly, the resemblance between CH_4 and $\Delta\varepsilon_{LAND}$ is not straightforward despite the fact that CH_4 is mainly driven by low latitude terrestrial emissions at least during glacial period (Loulergue, 2007). Over the last 350 ka, (i.e. period with higher resolution in the $\delta^{18}O_{atm}$ signal, enabling millennial variations to be resolved), the correlation is rather poor between CH_4 and $\delta^{18}O_{atm}$ ($R^2 = 0.20$) and between CH_4 and $\Delta\varepsilon_{LAND}$ ($R^2 = 0.35$). This is probably because CH_4 is not only sensitive to shifts of the ITCZ position, but also largely driven by high latitudes emissions especially during warm periods. As a conclusion, while $\Delta\varepsilon_{LAND}$ is appropriate to detect the drivers of $\delta^{18}O_{atm}$ changes during Heinrich events, it is not of much help on orbital timescale because of the strong influence of $\delta^{18}O_{sea\ water}$ whose relative chronology with respect to ice core chronologies is also uncertain.

4.3. Suggestions for the use of $\delta^{18}O_{atm}$ in ice core dating and application on the last glacial inception

Over the last 350 ka, where we have the highest resolution, there is clear evidence of millennial $\delta^{18}O_{atm}$ changes superimposed on $\delta^{18}O_{atm}$ variations resembling 65°N insolation. This is particularly visible over Termination III where the negative $\delta^{18}O_{atm}$ excursion, probably driven by insolation at 250 ka (Fig. 5 TIII-1), is interrupted by a positive excursion at 245 ka (Fig. 5 TIII-2) just before the strong characteristic decrease in $\delta^{18}O_{atm}$ of Termination III (Fig. 5 TIII-3). This feature can be generalized to each termination where Heinrich events are responsible for a significant increase in $\delta^{18}O_{atm}$, at the origin of a larger delay between summer insolation forcing and $\delta^{18}O_{atm}$ variations. The conclusion suggested by Fig. 5 is thus that the 5 ka delay between summer insolation forcing and $\delta^{18}O_{atm}$ variations used for ice core dating is mainly due to the occurrence of Heinrich events and hence especially valid for terminations. Consequently we propose that this 5 ka shift should not be systematically imposed for dating purposes using $\delta^{18}O_{atm}$ and July 21st insolation at 65°N and search for alternative tuning solutions.

Similarly to $\delta^{18}O_{atm}$, the East Asian $\delta^{18}O_{calcite}$ records are also influenced by millennial and orbital dynamics, high summer integrated insolation leading to lower $\delta^{18}O_{calcite}$ and southward shifts of the ITCZ concomitant with Heinrich events, leading to increases of $\delta^{18}O_{calcite}$. The common variations of $\delta^{18}O_{atm}$ and $\delta^{18}O_{calcite}$ are not unexpected. Using a modeling experiment, Reutenauer et al. (2015) clearly showed that the southward shift of the ITCZ, due to a North Atlantic freshwater flux designed to mimic a Heinrich event, leads to an increase of both $\delta^{18}O_{calcite}$ and $\delta^{18}O_{atm}$. It is thus tempting to use $\delta^{18}O_{calcite}$, integrating both millennial and orbital variations, as a target for the $\delta^{18}O_{atm}$ signal. Based on the above discussion, we argue that the choice of this target may be more correct than the July 21st insolation with a constant delay of 5 ka (or the June 21st insolation with a constant delay of 6 ka). Previous studies choose to align CH_4 with East Asian $\delta^{18}O_{calcite}$ speleothem (Shackleton et al., 2004; Buizert et al., 2015). While we recognize that this method may be appropriate for millennial events of the last glacial period, we argue for caution during deglaciations. Indeed, during the weak monsoon interval occurring within the first phase of a deglaciation marked by a Heinrich event, CH_4 shows a strong increase, probably induced by high latitude emissions. This CH_4 pattern during deglaciations disagrees with the $\delta^{18}O_{calcite}$ variations. Similarly, the orbital variations of the East Asian $\delta^{18}O_{calcite}$ are not seen in the CH_4 record probably due to high latitude emissions of CH_4 in the Northern hemisphere (e.g. Yu et al., 2013).

In Fig. 7, we display the phase delay (calculated with Match protocol) between the EDC $\delta^{18}O_{atm}$ record and the $\delta^{18}O_{calcite}$ stack for East Asian speleothems. In contrast to the difference between the orbitally tuned $\delta^{18}O_{atm}$ and $\delta O_2/N_2$ (Fig. 5) and despite chronological uncertainties, the delay between ice core $\delta^{18}O_{atm}$ and East Asian $\delta^{18}O_{calcite}$ does not exhibit systematic large values associated with terminations. Over the most recent period presenting a high-resolution $\delta^{18}O_{atm}$ record (last 350 ka), strong variations of the delay between ice core $\delta^{18}O_{atm}$ and East Asian $\delta^{18}O_{calcite}$ occur over MIS 5. We note that MIS 3, between 50 and 40 ka, is also associated with a high delay (~5 ka, Fig. 7). However, we refrain from discussing further this period because of the low correlation between the $\delta^{18}O_{atm}$ and $\delta^{18}O_{calcite}$ records (maximum $R^2 = 0.3$ against 0.7 for the whole 640 ka period), due to the multitude of rapid events recorded within the $\delta^{18}O_{calcite}$ record that cannot be captured accurately by $\delta^{18}O_{atm}$ due to the long residence time of oxygen.

In the following, we propose that aligning ice core $\delta^{18}O_{atm}$ and East Asian $\delta^{18}O_{calcite}$ can be a solution for improving ice core chronologies on long timescales and should replace the classical orbital alignment method. As a test for this new tuning method for $\delta^{18}O_{atm}$, we propose an application on the ice core MIS 5 chronology.

For this test, it should be stated that aligning $\delta^{18}O_{atm}$ and East Asian $\delta^{18}O_{calcite}$ is not always obvious because of the long residence time of oxygen in the atmosphere and the fact that $\delta^{18}O_{calcite}$ is sometimes showing abrupt variations, even during deglaciations or glacial inceptions. In a first attempt, we propose to align the $\delta^{18}O_{atm}$ and $\delta^{18}O_{calcite}$ records using mid-slopes of their variations. In other words, we align the extrema in the temporal derivatives of $\delta^{18}O_{atm}$ and $\delta^{18}O_{calcite}$ (Fig. 8). This exercise was done for the period 100–140 ka in order to propose an alternative timescale for the EDC and NGRIP ice cores, NGRIP and EDC chronologies being linked through stratigraphic dating constraints gathered in the AICC2012 chronology (Bazin et al., 2013; Veres et al., 2013). Other alignment methods between these records are presented in the section 4.4 dedicated to uncertainties.

Fig. 8 compares EDC $\delta^{18}O_{atm}$ with the East Asian $\delta^{18}O_{calcite}$ stack (as low latitude water cycle proxy) on one hand and NGRIP $\delta^{18}O_{ice}$ with $\delta^{18}O_{calcite}$ from NALPS (reflecting high latitudes northern hemisphere climate, Boch et al., 2011) on the other hand. As already noted in the introduction and in Veres et al. (2013), there is a clear mismatch between NGRIP $\delta^{18}O_{ice}$ and NALPS $\delta^{18}O_{calcite}$ over the last glacial inception when drawing NGRIP $\delta^{18}O_{ice}$ on the AICC2012 timescale. A similar mismatch is observed between EDC $\delta^{18}O_{atm}$

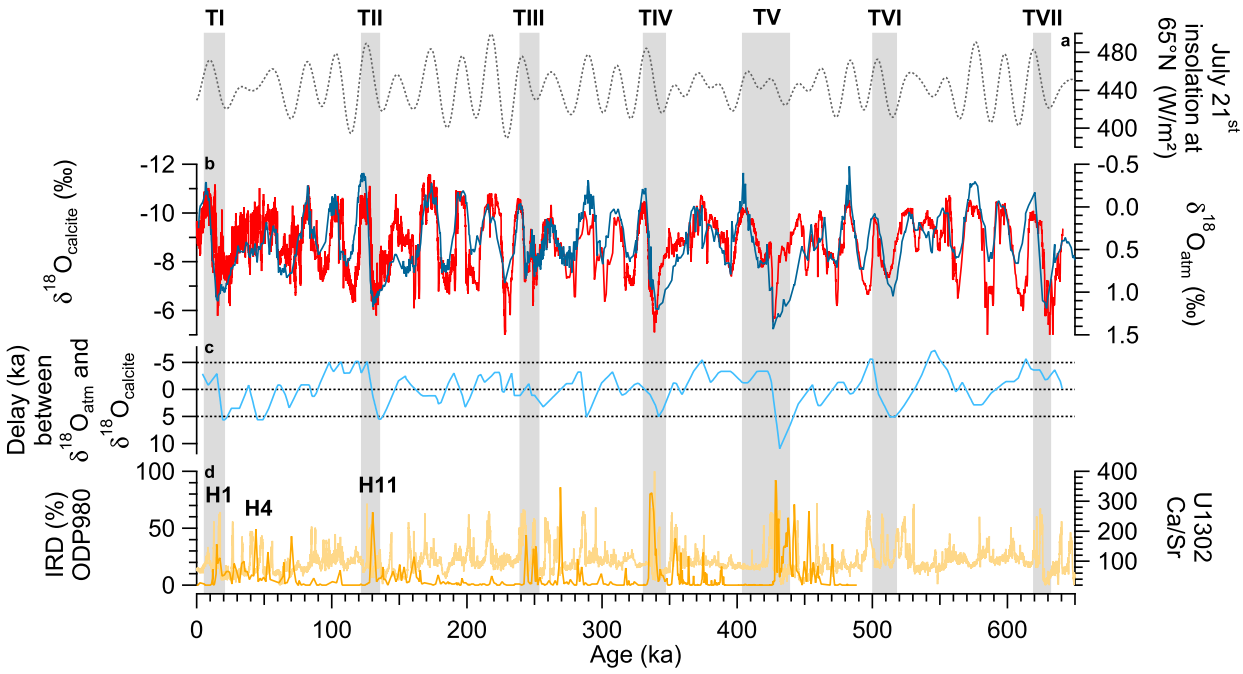

Fig. 7. a: July 21st insolation at 65°N (Laskar et al., 2004). b: The respective $\delta^{18}O_{atm}$ (blue: Petit et al., 1999; Dreyfus et al., 2007, 2008; Landais et al., 2013; Bazin et al., 2016; this study) and $\delta^{18}O_{calcite}$ (red: Cheng et al., 2016) records. c: Delay between ice core $\delta^{18}O_{atm}$ and $\delta^{18}O_{calcite}$ from Chinese caves. d: IRD percentage at site ODP980 (orange: McManus et al., 1999; Vazquez Riveiros, Comm. Pers.) and the Ca/Sr ratio at site U1302 (light orange: Channell et al., 2012). The line at 5 ka is the mean delay between the $\delta^{18}O_{atm}$ and the July 21st insolation at 65°N obtained during Terminations I and II. (For interpretation of the references to colour in this figure legend, the reader is referred to the Web version of this article.)

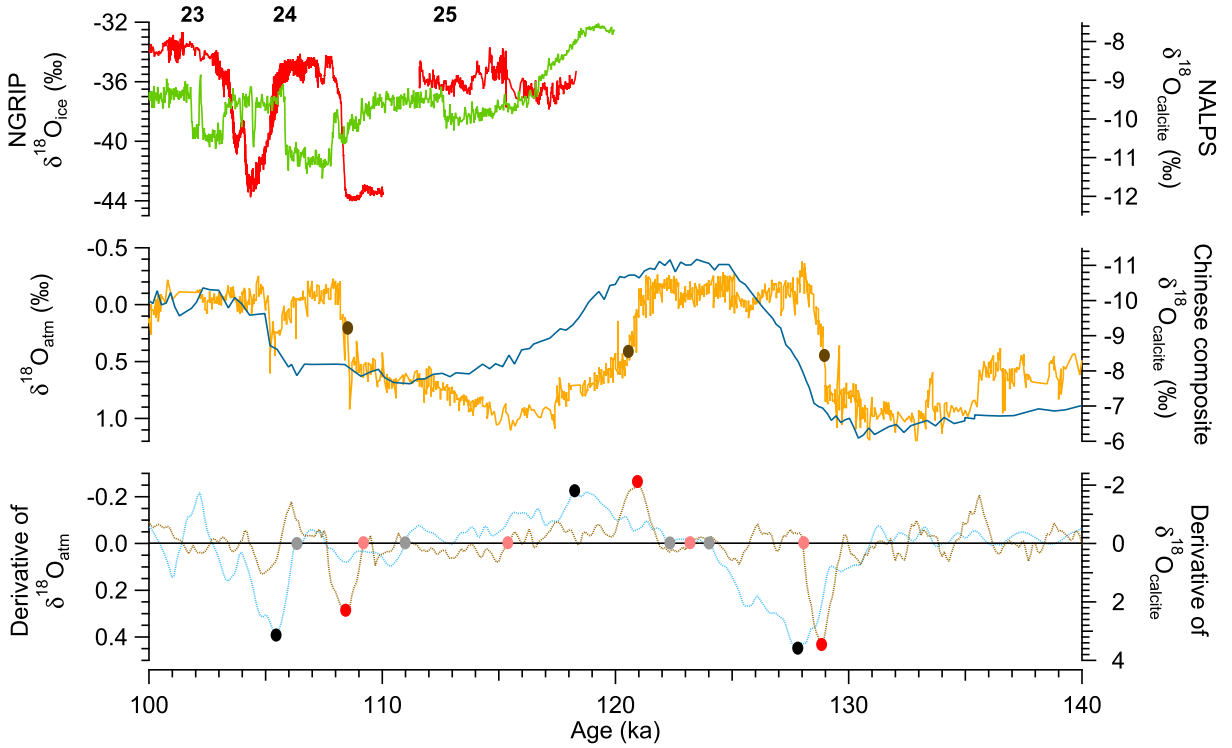

Fig. 8. Top: Comparison of high-mid latitude signals: NGRIP $\delta^{18}O_{ice}$ (green: NGRIP members, 2004) and NALPS speleothem $\delta^{18}O_{calcite}$ (red: Boch et al., 2011). Middle: Low latitude records: EDC $\delta^{18}O_{atm}$ (dark blue: Landais et al., 2013) and East Asian speleothem $\delta^{18}O_{calcite}$ (orange: Cheng et al., 2016). The brown dots represent the tie points used for the alignment between the extrema derivative of $\delta^{18}O_{atm}$ (black dots) and the abrupt changes in $\delta^{18}O_{calcite}$. Bottom: Time derivative of EDC $\delta^{18}O_{atm}$ (light blue) and East Asian $\delta^{18}O_{calcite}$ (brown) with indication of respective extrema (black and red dots) and change of sign (grey and pink dots) used to test the alignment method. The Dansgaard-Oeschger events are numbered. (For interpretation of the references to colour in this figure legend, the reader is referred to the Web version of this article.)

and East Asian $\delta^{18}O_{calcite}$ records. Even if shifts are expected between abrupt changes in surface temperature in Greenland and $\delta^{18}O_{calcite}$ in the Alps during the succession of Dansgaard-Oeschger (DO) events, a delay of 2.7 ka over the onset of DO 25 seems quite unrealistic (Fig. 8), given uncertainty of the NALPS chronology of 0.2–0.5 ka over the 60–120 ka period (Boch et al., 2011). Following our proposed alignment method between EDC $\delta^{18}O_{atm}$ and East Asian $\delta^{18}O_{calcite}$, we revise the EDC and NGRIP AICC2012 chronologies over this period using the Datice tool (Lemieux-Dudon et al., 2010; Bazin et al., 2013) using the new control points defined in Fig. 8 with a 1.22 ka uncertainty (chosen in agreement with uncertainties determined in section 4.4). All other stratigraphic and absolute control points used to constrain the coherent chronology between EDC, Vostok, EPICA Dronning Maud Land, TALDICE and NGRIP ice cores are the same as during the AICC2012 construction, except for the four Vostok $\delta^{18}O_{atm}$ age markers over MIS 5 that have been removed. We find an improved agreement between NGRIP $\delta^{18}O_{ice}$ on the revised chronology and NALPS $\delta^{18}O_{calcite}$, especially over the onset of DO 25, with a resulting chronology 2.2 ka older than AICC2012 (Fig. 9). The timing of DO 24 in NGRIP record is also 2.3 ka older than AICC2012 and is now comparable to the NALPS record. We thus consider the improved synchronization between NGRIP $\delta^{18}O_{ice}$ and NALPS $\delta^{18}O_{calcite}$ on Fig. 9 as encouraging for further use of East Asian $\delta^{18}O_{calcite}$ as target for $\delta^{18}O_{atm}$ dating.

4.4. Uncertainties and limitations

Even if alignment between $\delta^{18}O_{atm}$ and East Asian $\delta^{18}O_{calcite}$ may be a tool to refine ice core chronologies, we want to stress that it should not be used without cautiousness. First, the $\delta^{18}O_{atm}$ and $\delta^{18}O_{calcite}$ signals should be comparable on the considered periods. Second, even if modeling studies have confirmed the good correspondence between East Asian $\delta^{18}O_{calcite}$ and $\delta^{18}O_{atm}$ during Heinrich events (Reutenauer et al., 2015), the same demonstration needs to be done for orbital scales. Third, the match between $\delta^{18}O_{atm}$ and East Asian $\delta^{18}O_{calcite}$ is associated with three major sources of uncertainty detailed below.

1/ $\delta^{18}O_{atm}$ is a more integrative signal than East Asian $\delta^{18}O_{calcite}$ which involves large-scale atmospheric circulation effects but also a potential control of seasonality (sea surface temperature variation or ITCZ migration). However, Caley et al. (2014) have shown that the $\delta^{18}O_{calcite}$ has to be considered as a proxy of the mean annual hydrological cycle and not as a summer monsoonal proxy. They also estimate the uncertainty between summer and annual $\delta^{18}O_{calcite}$ variations in response to insolation forcing to about 1 ka. Taking into account a maximum 1 ka uncertainty, the $\delta^{18}O_{calcite}$ seems then a good proxy to infer annual variations of hydrological processes and comfort the suggestion of using it as a target for $\delta^{18}O_{atm}$ tuning.

2/ The uncertainties associated with the speleothems chronologies (obtained with ^{230}Th dating) need also to be considered. The different speleothems records in the composite signal of Cheng et al. (2016) have different uncertainties over the recent part. Wang et al. (2008) have obtained an uncertainty in age of ±0.7 ka (2σ) between 60 and 130 ka and ±1.5 ka (2σ) between 130 and 180 ka. Kelly et al. (2006) have an uncertainty of ~1 ka (2σ) between 100 and 140 ka and Dorale et al. (2004) have shown that for the last interglacial, the errors associated with ^{230}Th dating are ranging between 0.5 and 1 ka (2σ). So over the recent part of the East Asian $\delta^{18}O_{calcite}$ composite record, the uncertainty can be estimated to ~0.5 ka (1σ), but increases up to 8 ka at 640 ka (Cheng et al., 2016). This limits the alignment of $\delta^{18}O_{atm}$ with $\delta^{18}O_{calcite}$ for old time periods.

3/ In order to estimate the uncertainty related to the alignment method between the records, we test three different methods. First we choose to align both extrema in the time derivative corresponding to mid-slopes of $\delta^{18}O_{atm}$ and $\delta^{18}O_{calcite}$ records (Fig. 8). Second, we align periods where the sign of both derivatives are changing, corresponding to inflexion points in the $\delta^{18}O_{atm}$ and $\delta^{18}O_{calcite}$ original records (Fig. 8). Finally, we align the extrema values in the time derivative of $\delta^{18}O_{atm}$ and sharp changes in $\delta^{18}O_{calcite}$ (Fig. 8) since $\delta^{18}O_{atm}$ signal is an integrative signal on a much longer timescale than $\delta^{18}O_{calcite}$; this method is particularly well adapted for millennial variability. After realization of the different alignment methods and comparison of the resulting chronologies (Fig. 9), we estimate a maximum difference between the chronologies of 0.37 ka for DO 23, 0.44 ka for DO 24, and 0.40 ka for DO 25. Considering an upper limit for discrepancy between chronologies, we assign an additional 0.50 ka (1σ) uncertainty for the alignment method.

Finally, combining these three sources of uncertainties, we estimate a 1.22 ka (1σ) uncertainty for the $\delta^{18}O_{atm} - \delta^{18}O_{calcite}$ dating method over MIS 5.

4.5. Toward a new Antarctic ice core chronology

We apply here the new $\delta^{18}O_{atm}$ dating approach for the EDC ice

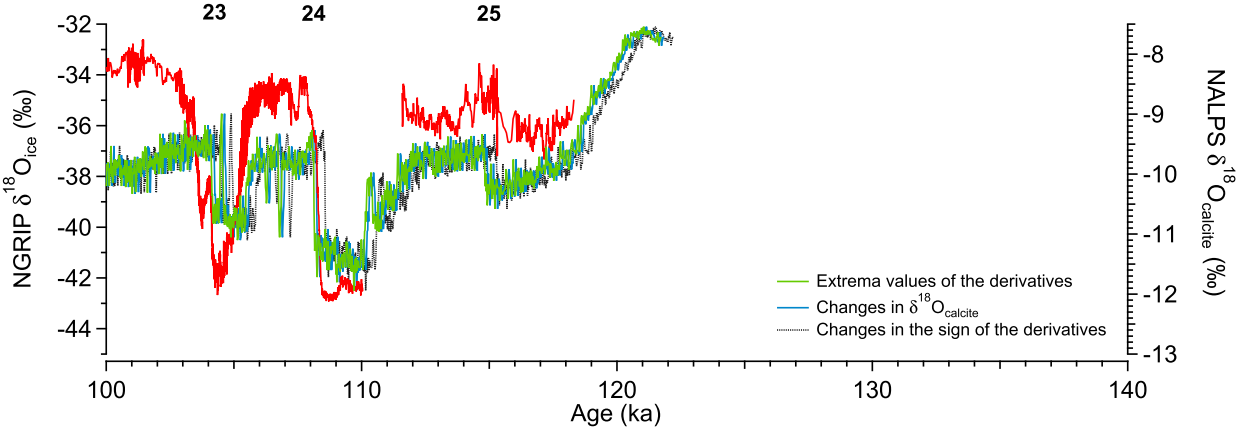

Fig. 9. NALPS speleothem $\delta^{18}O_{calcite}$ record (red: Boch et al., 2011) and NGRIP $\delta^{18}O_{ice}$ evolution on the new chronologies after aligning $\delta^{18}O_{atm}$ and East Asian $\delta^{18}O_{calcite}$ based on the extrema values of the derivatives (green curve), the extrema values of the $\delta^{18}O_{atm}$ derivative with changes in $\delta^{18}O_{calcite}$ (blue curve), and change of the derivatives sign (dashed black curve). The Dansgaard-Oeschger events are numbered. (For interpretation of the references to colour in this figure legend, the reader is referred to the Web version of this article.)

core over the 100–640 ka period where alignment with speleothems could potentially reduce the current uncertainty in EDC chronology. Using the same methodology as presented in section 4.3, we chose 51 markers between 100 and 640 ka (corresponding to the extrema values of the time derivative) to align the $\delta^{18}O_{atm}$ and the $\delta^{18}O_{calcite}$ signals (Fig. 10). Over this time period, the uncertainties associated with speleothems ^{230}Th dating are taken from Cheng et al. (2016). We additionally consider a 1 ka uncertainty for the $\delta^{18}O_{calcite}$ variations in response to insolation forcing and a 0.5 ka uncertainty for the $\delta^{18}O_{atm} - \delta^{18}O_{calcite}$ alignment method as discussed in previous section. The total uncertainties can then be calculated and applied between 100 and 640 ka. They vary between 1.3 ka at 105 ka to 6.9 ka at 630 ka. Before 640 ka, in the absence of speleothem data, we kept the classical $\delta^{18}O_{atm}$ orbital tuning to precession with an uncertainty of 6 ka as used for AICC2012.

Fig. 10 compares the EDC δD record on AICC2012 and on the new chronology based on the $\delta^{18}O_{atm} - \delta^{18}O_{calcite}$ alignment method. The difference between the two chronologies is generally below 2 ka except for the last glacial inception and over the sequence of MIS 10 and MIS 11 where differences up to 4 ka are reached. In particular, taking the classical threshold of −403‰ as a definition of an Antarctic warm period (EPICA community members, 2004), the MIS 11 duration is only 29.8 ka on the $\delta^{18}O_{atm} - \delta^{18}O_{calcite}$ chronology compared to the 31.1 ka estimated on AICC2012. Most importantly, the age uncertainty is strongly reduced around MIS 11 in the chronology based on the $\delta^{18}O_{atm} - \delta^{18}O_{calcite}$ alignment with a reduction from 3.8 ka for AICC2012 to 2.3 ka (Fig. 10). Indeed, due to low eccentricity, only few orbital tie points could be found over this period during the construction of AICC2012 as can be seen from the poor correspondence between $\delta^{18}O_{atm}$ ($\delta O_2/N_2$) and summer insolation at 65°N (December 21st insolation at 75°S) on Fig. 5. The matching between $\delta^{18}O_{atm}$ and $\delta^{18}O_{calcite}$ over the MIS 10 – MIS 11 period (Appendix C) is much better than the matching between $\delta^{18}O_{atm}$ and summer insolation. Before 450 ka and due to higher speleothem dating uncertainties, the $\delta^{18}O_{atm} - \delta^{18}O_{calcite}$ chronology present higher uncertainties, close to the ones obtained with the AICC2012 chronology (Fig. 10).

5. Summary & conclusions

In this study we have presented new EDC $\delta^{18}O_{atm}$ data between 153 and 374 ka expanding the previous EDC record focused on the 300–800 ka and 100–150 ka periods. The high-resolution record presented here allows an unprecedented study of $\delta^{18}O_{atm}$ dynamics over the recent glacial terminations. These data were combined with new $\delta O_2/N_2$ data obtained on well-preserved ice (−50 °C) for the same period. Combination of these series on the same ice core shows that the classical dating target for $\delta^{18}O_{atm}$, i.e. the boreal summer insolation with a constant 5 ka shift, should be revised. Indeed, we show that this 5 ka shift is mainly due to the delay induced by Heinrich events particularly during deglaciations. As already demonstrated in previous studies (e.g. Landais et al., 2007; Severinghaus et al., 2009; Capron et al., 2012), $\delta^{18}O_{atm}$ is sensitive to both orbital and millennial scale variations of the low latitude water cycle.

Because East Asian $\delta^{18}O_{calcite}$ includes similar orbital and millennial variations, and is also directly influenced by the low latitude water cycle, we propose that East Asian $\delta^{18}O_{calcite}$ could be used as an alternative target for the $\delta^{18}O_{atm}$ signal because of their concomitant variations. This is especially true over Heinrich events associated with Weak Monsoon Interval through a southward shift of the ITCZ. We argue that matching $\delta^{18}O_{atm}$ with East Asian $\delta^{18}O_{calcite}$ is probably a better tool for ice core dating than the matching of CH_4 to East Asian $\delta^{18}O_{calcite}$ during glacial-interglacial transitions. Indeed, while methane shares many similarities with

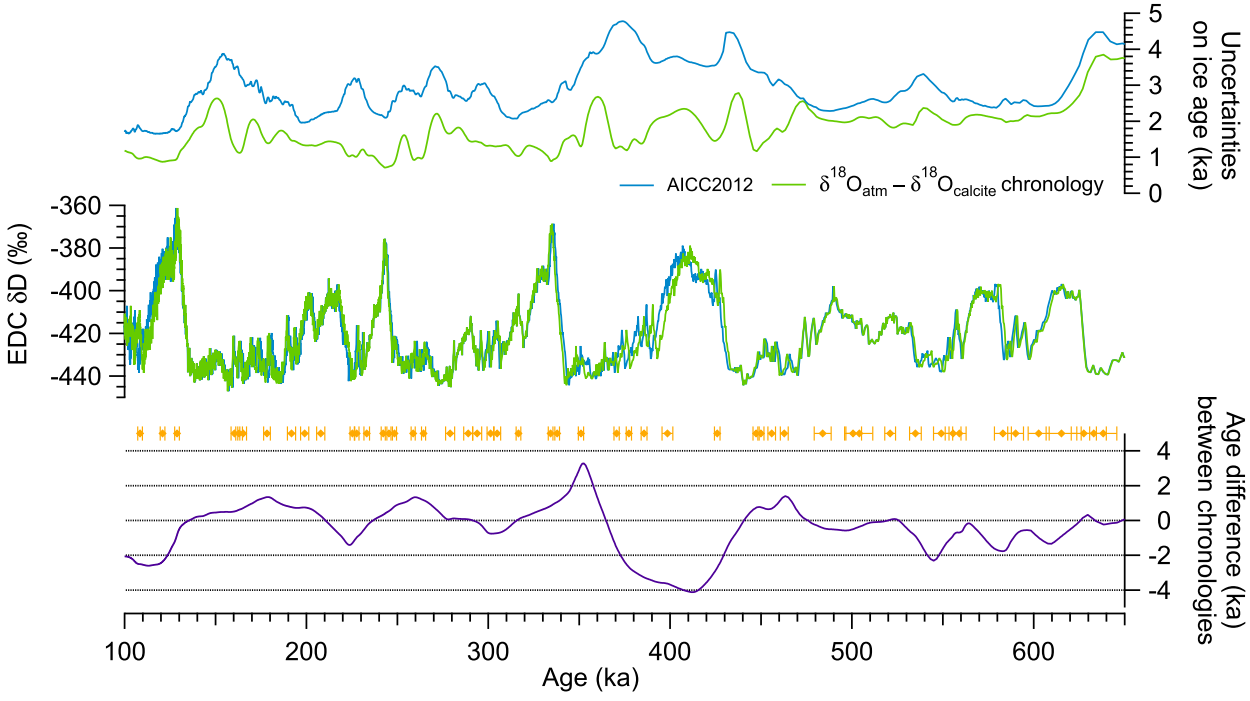

Fig. 10. Top: Representation of the uncertainties associated with the ice age of AICC2012 (blue: Bazin et al., 2013) and $\delta^{18}O_{atm} - \delta^{18}O_{calcite}$ (green) chronologies. Middle: δD evolution between 100 and 640 ka on AICC2012 (blue: Jouzel et al., 2007) and on the new EDC chronology (green). The orange diamonds represent the markers used for the alignment between $\delta^{18}O_{atm}$ and $\delta^{18}O_{calcite}$. Bottom: The age difference between AICC2012 and the $\delta^{18}O_{atm} - \delta^{18}O_{calcite}$ chronology is represented. (For interpretation of the references to colour in this figure legend, the reader is referred to the Web version of this article.)

$\delta^{18}O_{calcite}$ during millennial scale variability of the last glacial period, methane variations do not exhibit similar variations to $\delta^{18}O_{calcite}$ over deglaciation and some precession cycle. This is probably because methane is strongly influenced by high latitude emissions during warm periods while $\delta^{18}O_{atm}$ is more sensitive to low latitude water cycle.

Finally, this new dating strategy has been tested over the last glacial inception where the alignment between $\delta^{18}O_{atm}$ and East Asian $\delta^{18}O_{calcite}$ leads to an improved comparison between NGRIP $\delta^{18}O_{ice}$ record and mid-latitude climatic record (here NALPS speleothems). It was then extended to the last 640 ka where the new chronology based on $\delta^{18}O_{atm} - \delta^{18}O_{calcite}$ alignment implies revised ages, in particular for duration of MIS 11. The uncertainty of the chronology based on $\delta^{18}O_{atm} - \delta^{18}O_{calcite}$ alignment is significantly reduced (~2 ka instead of ~4 ka) around MIS 11, hence supporting further use of this dating tool for future ice core dating.

Still, it could be argued that there is yet no direct proof that $\delta^{18}O_{atm}$ is varying synchronously with East Asian climatic signal and hence $\delta^{18}O_{calcite}$ on long timescales. This is the reason why, following the model study of $\delta^{18}O_{atm}$ over a Heinrich event (Reutenauer et al., 2015), we see as a next step the direct simulation of both $\delta^{18}O_{calcite}$ and $\delta^{18}O_{atm}$ over at least one climatic cycle.

Acknowledgments

We acknowledge Alexandre Cauquoin for his contribution to the Match protocol learning. We thank Frédéric Parrenin, Jai Chowdhry Beeman, Bruno Malaizé and Louis Francois for fruitful discussions. We also thank the glaciological program of the French Polar Institute (IPEV) and Catherine Ritz involved in cutting EDC $\delta O_2/N_2$ samples. It is a contribution to the European Project for Ice Coring in Antarctica (EPICA). This work was supported by Labex L-IPSL, which is funded by the ANR (grant no. ANR-10-LABX-0018) as well as the Belmont Forum's Pacmedy project.

Appendix A. $\delta^{18}O_{atm}$ and $\delta O_2/N_2$ relationship

Gas loss during storage at −20 °C has the effect to decrease the O_2/N_2 ratio, since O_2 molecules are smaller than N_2 molecules. It also affects the $\delta^{18}O$ of O_2 in air trapped in ice core and hence $\delta^{18}O_{atm}$. Landais et al. (2003b) have found a linear relationship of 0.01 due to gas loss between the changes in $\delta O_2/N_2$ and changes in $\delta^{18}O_{atm}$ in the Vostok and GRIP ice cores. This relationship is in good agreement with the link between $\delta^{18}O_{atm}$ and $\delta O_2/N_2$ variations found by Severinghaus et al. (2009) for the Siple Dome ice core even if these authors also used the Ar/N_2 ratio to better constrain gas loss effects.

In our study, Ar/N_2 measurements could not be determined with a sufficient precision. We thus used $\delta^{18}O_{atm}$ and $\delta O_2/N_2$ measurements presenting large differences between the $\delta O_2/N_2$ replicate values to study the relationship between these two proxies. We did this exercise for two datasets, 2014 and 2015–2016, and plot the difference between $\delta^{18}O_{atm}$ replicates versus the difference between $\delta O_2/N_2$ replicates of the same sample on Fig. A1. We obtain a mean slope of 0.012 (Fig. A1), which is coherent with the slope of 0.01 found by Landais et al. (2003b) for the relationship between $\delta^{18}O_{atm}$ and $\delta O_2/N_2$ due to gas loss and we thus choose to apply the same correction:

$$\delta^{18}O_{atm\ corrected} = \delta^{18}O_{atm} + (\delta O_2/N_2 + 10) \times 0.01 \quad (A1)$$

The average value of −10‰ in the above equation agrees with the mean value of the $\delta O_2/N_2$ signal at EDC without gas loss influence over our series of measurements.

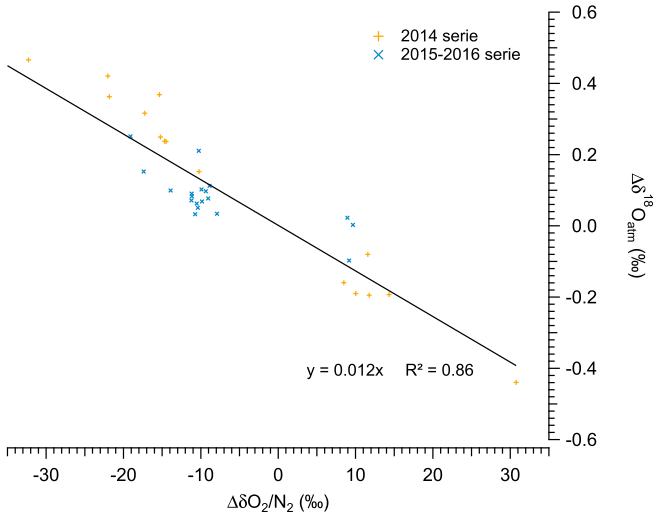

Fig. A1. Paired difference plot for the $\delta^{18}O_{atm}$ versus $\delta O_2/N_2$ (second replicate minus first replicate) for two datasets: 2014 in orange and 2015–2016 in blue.

Appendix B. $\Delta\varepsilon_{LAND}$ calculation

$\Delta\varepsilon_{LAND}$ is an empirical parameter that represents the water cycle and respiratory fractionation changes over time (Severinghaus et al., 2009). This parameter is calculated using the following equation:

$$\Delta\varepsilon_{LAND} = \left[\tau \times \frac{d\delta^{18}O_{atm}}{dt} + \delta^{18}O_{atm} - \delta^{18}O_{sea\ water}\right] \times \frac{1}{f_L} \quad (B1)$$

where τ is the residence time of oxygen in the atmosphere (1 ka), $d\delta^{18}O_{atm}/dt$ is the temporal derivative of $\delta^{18}O_{atm}$, $\delta^{18}O_{sea\ water}$ is the global isotopic composition of sea water, whose evolution over the last climatic cycles can be obtained from Lisiecki and Raymo (2005), and f_L is the fraction of oxygen photosynthesis occurring on land (consider constant in time and equal to 0.65 based on the discussion by Blunier et al., 2002). To calculate $\Delta\varepsilon_{LAND}$, the $\delta^{18}O_{atm}$ series was interpolated with a 100 years' time step and then fitted using the Savitzky-Golay algorithm with 25 points at second order. The time derivative was then calculated on this fitted curve using the $\delta^{18}O_{atm}$ slope over a 200 years period. The $\delta^{18}O_{sea\ water}$ record has also been interpolated with a 100 years' time step and smoothed with the Savitzky-Golay algorithm to match the $\delta^{18}O_{atm}$ timescale. Finally, the $\Delta\varepsilon_{LAND}$ has been calculated using the time derivative and the corresponding smoothed and interpolated $\delta^{18}O$ values.

Appendix C. $\delta^{18}O_{atm}$ chronology comparison

Fig. C1 shows how the new chronology improves the correlation between $\delta^{18}O_{atm}$ and $\delta^{18}O_{calcite}$ especially during periods where the delay was maximum in Fig. 7 (e.g. R^2 increases from 0.49 to 0.76 for Termination II and from 0.53 to 0.75 during MIS 10–11).

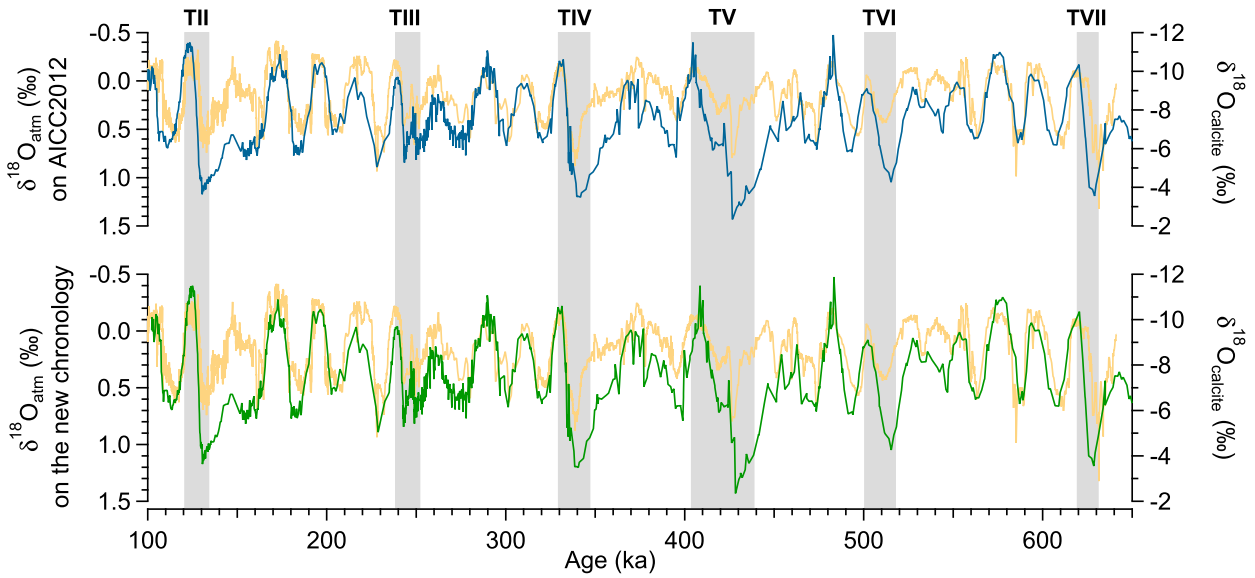

Fig. C1. Comparison of $\delta^{18}O_{calcite}$ from East Asian speleothems (orange: Cheng et al., 2016) with the $\delta^{18}O_{atm}$ record on AICC2012 in blue (Dreyfus et al., 2007, 2008; Landais et al., 2013; Bazin et al., 2016; this study) and on the $\delta^{18}O_{atm} - \delta^{18}O_{calcite}$ chronology in green.

References

Battle, M., Bender, M., Sowers, T., Tans, P.P., Butler, J.H., Elkins, J.W., Ellis, J.T., Conway, T., Zhang, N., Lang, P., Clarket, A.D., 1996. Atmospheric gas concentrations over the past century measured in air from firn at the South Pole. Nature 383, 231–235. https://doi.org/10.1038/383231a0.

Bazin, L., Landais, A., Lemieux-Dudon, B., Toyé Mahamadou Kele, H., Veres, D., Parrenin, F., Martinerie, P., Ritz, C., Capron, E., Lipenkov, V., Loutre, M.-F., Raynaud, D., Vinther, B., Svensson, A., Rasmussen, S.O., Severi, M., Blunier, T., Leuenberger, M., Fischer, H., Masson-Delmotte, V., Chappellaz, J., Wolff, E., 2013. An optimized multi-proxy, multi-site Antarctic ice and gas orbital chronology (AICC2012): 120-800 ka. Clim. Past 9, 1715–1731. https://doi.org/10.5194/cp-9-1715-2013.

Bazin, L., Landais, A., Capron, E., Masson-Delmotte, V., Ritz, C., Picard, G., Jouzel, J., Dumont, M., Leuenberger, M., Prié, F., 2016. Phase relationships between orbital forcing and the composition of air trapped in Antarctic ice cores. Clim. Past 12, 729–748. https://doi.org/10.5194/cp-12-729-2016.

Bender, M.L., Sowers, T., Labeyrie, L., 1994. The Dole effect and its variations during the last 130,000 years as measured in the Vostok ice core. Global Biogeochem. Cycles 8, 363–376. https://doi.org/10.1029/94GB00724.

Bender, M.L., 2002. Orbital tuning chronology for the Vostok climate record supported by trapped gas composition. Earth Planet Sci. Lett. 204, 275–289. https://doi.org/10.1016/S0012-821X(02)00980-9.

Bintanja, R., van de Wal, R.S.W., Oerlemans, J., 2005. Modelled atmospheric temperatures and global sea levels over the past million years. Nature 437, 125–128. https://doi.org/10.1038/nature03975.

Blunier, T., Barnett, B., Bender, M.L., Hendricks, M.B., 2002. Biological oxygen productivity during the last 60,000 years from triple oxygen isotope measurements. Global Biogeochem. Cycles 16 (3). https://doi.org/10.1029/2001GB001460.

Boch, R., Cheng, H., Spötl, C., Edwards, R.L., Wang, X., Häuselmann, P., 2011. NALPS: a precisely dated European climate record 120–60 ka. Clim. Past 7, 1247–1259. https://doi.org/10.5194/cp-7-1247-2011.

Bréant, C., Martinerie, P., Orsi, A., Arnaud, L., Landais, A., 2017. Modelling firn thickness evolution during the last deglaciation: constraints on sensitivity to temperature and impurities. Clim. Past 13, 833–853. https://doi.org/10.5194/cp-13-833-2017.

Buizert, C., Cuffey, K.M., Severinghaus, J.P., Baggenstos, D., Fudge, T.J., Steig, E.J., Markle, B.R., Winstrup, M., Rhodes, R.H., Brook, E.J., Sowers, T.A., Clow, G.D., Cheng, H., Edwards, R.L., Sigl, M., McConnell, J.R., Taylor, K.C., 2015. The WAIS Divide deep ice core WD2014 chronology – Part 1: methane synchronization (68–31 ka BP) and the gas age–ice age difference. Clim. Past 11, 153–173. https://doi.org/10.5194/cp-11-153-2015.

Caley, T., Roche, D.M., Renssen, H., 2014. Orbital Asian summer monsoon dynamics revealed using an isotope-enabled global climate model. Nat. Commun. 5 (5371). https://doi.org/10.1038/ncomms6371.

Capron, E., Landais, A., Lemieux-Dudon, B., Schilt, A., Masson-Delmotte, V., Buiron, D., Chappellaz, J., Dahl-Jensen, D., Johnsen, S., Leuenberger, M., Loulergue, L., Oerter, H., 2010. Synchronising EDML and NorthGRIP ice cores using $\delta^{18}O$ of atmospheric oxygen ($\delta^{18}O_{atm}$) and CH_4 measurements over MIS5 (80–123 kyr). Quat. Sci. Rev. 29, 222–234. https://doi.org/10.1016/j.quascirev.2009.07.014.

Capron, E., Landais, A., Chappellaz, J., Buiron, D., Fischer, H., Johnsen, S.J., Jouzel, J., Leuenberger, M., Masson-Delmotte, V., Stocker, T.F., 2012. A global picture of the first abrupt climatic event occurring during the last glacial inception. Geophys. Res. Lett. 39. https://doi.org/10.1029/2012GL052656.

Channell, J.E.T., Hodell, D.A., Romero, O., Hillaire-Marcel, C., de Vernal, A., Stoner, J.S., Mazaud, A., Röhl, U., 2012. A 750-kyr detrital-layer stratigraphy for the North Atlantic (IODP sites U1302–U1303, Orphan Knoll, Labrador sea). Earth Planet Sci. Lett. 317–318, 218–230. https://doi.org/10.1016/j.epsl.2011.11.029.

Cheng, H., Edwards, R.L., Sinha, A., Spötl, C., Yi, L., Chen, S., Kelly, M., Kathayat, G., Wang, X., Li, X., Kong, X., Wang, Y., Ning, Y., Zhang, H., 2016. The Asian monsoon over the past 640,000 years and ice age terminations. Nature 534, 640–646. https://doi.org/10.1038/nature18591.

Clemens, S.C., Prell, W.L., Sun, Y., 2010. Orbital-scale timing and mechanisms driving Late Pleistocene Indo-Asian summer monsoons: reinterpreting cave speleothem δ18O. Paleoceanography 25. https://doi.org/10.1029/2010PA001926.

Craig, H., Horibe, Y., Sowers, T., 1988. Gravitational separation of gases and isotopes in polar ice caps. Science 242, 1675–1678. https://doi.org/10.1126/science.242.4886.1675.

Dorale, J.A., Edwards, R.L., Alexander, E.C., Shen, C.-C., Richards, D.A., Cheng, H., 2004. Uranium-series dating of speleothems: current techniques, limits, & applications. In: Sasowsky, I.D., Mylroie, J. (Eds.), Studies of Cave Sediments. Springer, Boston, MA, pp. 177–197. https://doi.org/10.1007/978-1-4419-9118-8_10.

Dreyfus, G.B., Parrenin, F., Lemieux-Dudon, B., Durand, G., Masson-Delmotte, V., Jouzel, J., Barnola, J.-M., Panno, L., Spahni, R., Tisserand, A., Siegenthaler, U., Leuenberger, M., 2007. Anomalous flow below 2700 m in the EPICA Dome C ice core detected using $\delta^{18}O$ of atmospheric oxygen measurements. Clim. Past 3, 341–353. https://doi.org/10.5194/cp-3-341-2007.

Dreyfus, G.B., 2008. Dating an 800,000 Year Antarctic Ice Core Record Using the Isotopic Composition of Trapped Air. PhD thesis. Princeton University.

Dreyfus, G.B., Raisbeck, G.M., Parrenin, F., Jouzel, J., Guyodo, Y., Nomade, S., Mazaud, A., 2008. An ice core perspective on the age of the Matuyama–Brunhes boundary. Earth Planet Sci. Lett. 274, 151–156. https://doi.org/10.1016/j.epsl.2008.07.008.

Dreyfus, G.B., Jouzel, J., Bender, M.L., Landais, A., Masson-Delmotte, V., Leuenberger, M., 2010. Firn processes and $\delta^{15}N$: potential for a gas-phase climate proxy. Quat. Sci. Rev. 29, 28–42. https://doi.org/10.1016/j.quascirev.2009.10.012.

EPICA community members, 2004. Eight glacial cycles from an Antarctic ice core. Nature 429, 623–628.

Fujita, S., Okuyama, J., Hori, A., Hondoh, T., 2009. Metamorphism of stratified firn at Dome Fuji, Antarctica: a mechanism for local insolation modulation of gas transport conditions during bubble close off. J. Geophys. Res. 114. https://doi.org/10.1029/2008JF001143.

Fujita, S., Parrenin, F., Severi, M., Motoyama, H., Wolff, E.W., 2015. Volcanic synchronization of Dome Fuji and Dome C Antarctic deep ice cores over the past 216 kyr. Clim. Past 11, 1395–1416. https://doi.org/10.5194/cp-11-1395-2015.

Goujon, C., Barnola, J.-M., Ritz, C., 2003. Modeling the densification of polar firn including heat diffusion: application to close-off characteristics and gas isotopic fractionation for Antarctica and Greenland sites. J. Geophys. Res. Atmospheres 108. D24, 4792. https://doi.org/10.1029/2002JD003319.

Huber, C., Beyerle, U., Leuenberger, M., Schwander, J., Kipfer, R., Spahni, R., Severinghaus, J., Weiler, K., 2006. Evidence for molecular size dependent gas fractionation in firn air derived from noble gases, oxygen, and nitrogen measurements. Earth Planet Sci. Lett. 243, 61–73. https://doi.org/10.1016/j.epsl.2005.12.036.

Hutterli, M.A., Schneebeli, M., Freitag, J., Kipfstuhl, J., Rothlisberger, R., 2010. Impact of Local Insolation on Snow Metamorphism and Ice Core Records. Hokkaido Univ. Press Sapporo Japan, pp. 223–232.

Jouzel, J., Waelbroeck, C., Malaizé, B., Bender, M., Petit, J.R., Stievenard, M., Barkov, N.I., Barnola, J.M., King, T., Kotlyakov, V.M., Lipenkov, V., Lorius, C., Raynaud, D., Sowers, T., 1996. Climatic interpretation of the recently extended Vostok ice records. Clim. Dynam. 12, 513–521.

Jouzel, J., Hoffmann, G., Parrenin, F., Waelbroeck, C., 2002. Atmospheric oxygen 18 and sea-level changes. Quat. Sci. Rev. 21, 307–314. https://doi.org/10.1016/S0277-3791(01)00106-8.

Jouzel, J., Masson-Delmotte, V., Cattani, O., Dreyfus, G., Falourd, S., Hoffmann, G., Minster, B., Nouet, J., Barnola, J.M., Chappellaz, J., Fischer, H., Gallet, J.C., Johnsen, S., Leuenberger, M., Loulergue, L., Luethi, D., Oerter, H., Parrenin, F., Raisbeck, G., Raynaud, D., Schilt, A., Schwander, J., Selmo, E., Souchez, R., Spahni, R., Stauffer, B., Steffensen, J.P., Stenni, B., Stocker, T.F., Tison, J.L., Werner, M., Wolff, E.W., 2007. Orbital and millennial Antarctic climate variability over the past 800,000 years. Science 317, 793–796. https://doi.org/10.1126/science.1141038.

Kawamura, K., Parrenin, F., Lisiecki, L., Uemura, R., Vimeux, F., Severinghaus, J.P., Hutterli, M.A., Nakazawa, T., Aoki, S., Jouzel, J., Raymo, M.E., Matsumoto, K., Nakata, H., Motoyama, H., Fujita, S., Goto-Azuma, K., Fujii, Y., Watanabe, O., 2007. Northern Hemisphere forcing of climatic cycles in Antarctica over the past 360,000 years. Nature 448, 912–916. https://doi.org/10.1038/nature06015.

Kelly, M.J., Edwards, R.L., Cheng, H., Yuan, D., Cai, Y., Zhang, M., Lin, Y., An, Z., 2006. High resolution characterization of the Asian Monsoon between 146,000 and 99,000 years B.P. from Dongge Cave, China and global correlation of events surrounding Termination II. Palaeogeogr. Palaeoclimatol. Palaeoecol. 236, 20–38. https://doi.org/10.1016/j.palaeo.2005.11.042.

Landais, A., Caillon, N., Severinghaus, J.P., Jouzel, J., Masson-Delmotte, V., 2003a. Analyses isotopiques à haute précision de l'air piégé dans les glaces polaires pour la quantification des variations rapides de température: méthodes et limites. Notes des activités instrumentales de l'IPSL 39.

Landais, A., Chappellaz, J., Delmotte, M., Jouzel, J., Blunier, T., Bourg, C., Caillon, N., Cherrier, S., Malaizé, B., Masson-Delmotte, V., Raynaud, D., Schwander, J., Steffensen, J.P., 2003b. A tentative reconstruction of the last interglacial and glacial inception in Greenland based on new gas measurements in the Greenland Ice Core Project (GRIP) ice core. J. Geophys. Res. 108. https://doi.org/10.1029/2002JD003147.

Landais, A., Masson-Delmotte, V., Combourieu Nebout, N., Jouzel, J., Blunier, T., Leuenberger, M., Dahl-Jensen, D., Johnsen, S., 2007. Millennial scale variations of the isotopic composition of atmospheric oxygen over Marine Isotopic Stage 4. Earth Planet Sci. Lett. 258, 101–113. https://doi.org/10.1016/j.epsl.2007.03.027.

Landais, A., Dreyfus, G., Capron, E., Masson-Delmotte, V., Sanchez-Goñi, M.F., Desprat, S., Hoffmann, G., Jouzel, J., Leuenberger, M., Johnsen, S., 2010. What drives the millennial and orbital variations of δ^{18}Oatm? Quat. Sci. Rev. 29, 235–246. https://doi.org/10.1016/j.quascirev.2009.07.005.

Landais, A., Dreyfus, G., Capron, E., Pol, K., Loutre, M.F., Raynaud, D., Lipenkov, V.Y., Arnaud, L., Masson-Delmotte, V., Paillard, D., Jouzel, J., Leuenberger, M., 2012. Towards orbital dating of the EPICA Dome C ice core using $\delta O_2/N_2$. Clim. Past 8, 191–203. https://doi.org/10.5194/cp-8-191-2012.

Landais, A., Dreyfus, G., Capron, E., Jouzel, J., Masson-Delmotte, V., Roche, D.M., Prié, F., Caillon, N., Chappellaz, J., Leuenberger, M., Lourantou, A., Parrenin, F., Raynaud, D., Teste, G., 2013. Two-phase change in CO_2, Antarctic temperature and global climate during Termination II. Nat. Geosci. 6, 1062–1065. https://doi.org/10.1038/ngeo1985.

Laskar, J., Robutel, P., Joutel, F., Gastineau, M., Correia, A.C.M., Levrard, B., 2004. A long-term numerical solution for the insolation quantities of the Earth. Astron. Astrophys 428, 261–285. https://doi.org/10.1051/0004-6361, 20041335.

Lemieux-Dudon, B., Blayo, E., Petit, J.-R., Waelbroeck, C., Svensson, A., Ritz, C., Barnola, J.-M., Narcisi, B.M., Parrenin, F., 2010. Consistent dating for Antarctic and Greenland ice cores. Quat. Sci. Rev. 29, 8–20. https://doi.org/10.1016/j.quascirev.2009.11.010.

Lisiecki, L.E., Lisiecki, P.A., 2002. Application of dynamic programming to the correlation of paleoclimate records. Paleoceanography 17. https://doi.org/10.1029/2001PA000733.

Lisiecki, L.E., Raymo, M.E., 2005. A Pliocene-Pleistocene stack of 57 globally distributed benthic δ^{18}O records. Paleoceanography 20. https://doi.org/10.1029/2004PA001071.

Loulergue, L., 2007. Contraintes chronologiques et biogéochimiques grâce au méthane dans la glace naturelle: une application aux forages du projet EPICA. PhD thesis. Université Joseph-Fourier-Grenoble I.

Loulergue, L., Schilt, A., Spahni, R., Masson-Delmotte, V., Blunier, T., Lemieux, B., Barnola, J.-M., Raynaud, D., Stocker, T.F., Chappellaz, J., 2008. Orbital and millennial-scale features of atmospheric CH_4 over the past 800,000 years. Nature 453, 383–386. https://doi.org/10.1038/nature06950.

Lüthi, D., Le Floch, M., Bereiter, B., Blunier, T., Barnola, J.-M., Siegenthaler, U., Raynaud, D., Jouzel, J., Fischer, H., Kawamura, K., Stocker, T.F., 2008. High-resolution carbon dioxide concentration record 650,000–800,000 years before present. Nature 453, 379–382. https://doi.org/10.1038/nature06949.

Malaizé, B., Paillard, D., Jouzel, J., Raynaud, D., 1999. The Dole effect over the last two glacial-interglacial cycles. J. Geophys. Res. Atmospheres 104, 14199–14208. https://doi.org/10.1029/1999JD900116.

McManus, J.F., Oppo, D.W., Cullen, J.L., 1999. A 0.5-million-year record of millennial-scale climate variability in the North Atlantic. Science 283, 971–975.

NorthGRIP members, 2004. High resolution climate record of the northern hemisphere reaching into the last glacial interglacial period. Nature 431, 147–151.

Parrenin, F., Barnola, J.-M., Beer, J., Blunier, T., Castellano, E., Chappellaz, J., Dreyfus, G., Fischer, H., Fujita, S., Jouzel, J., Kawamura, K., Lemieux-Dudon, B., Loulergue, L., Masson-Delmotte, V., Narcisi, B., Petit, J.-R., Raisbeck, G., Raynaud, D., Ruth, U., Schwander, J., Severi, M., Spahni, R., Steffensen, J.P., Svensson, A., Udisti, R., Waelbroeck, C., Wolff, E., 2007. The EDC3 chronology for the EPICA Dome C ice core. Clim. Past 3, 485–497.

Petit, J.-R., Jouzel, J., Raynaud, D., Barkov, N.I., Barnola, J.-M., Basile, I., Bender, M.L., Chappellaz, J., Davis, M., Delaygue, G., Delmotte, M., Kotlyakov, V.M., Lorius, C., Pepin, L., Ritz, C., Saltzman, E., Stievenard, M., 1999. Climate and atmospheric history of the past 420,000 years from the Vostok ice core, Antarctica. Nature 399, 429–436.

Raynaud, D., Lipenkov, V., Lemieux-Dudon, B., Duval, P., Loutre, M.-F., Lhomme, N., 2007. The local insolation signature of air content in Antarctic ice. A new step toward an absolute dating of ice records. Earth Planet Sci. Lett. 261, 337–349. https://doi.org/10.1016/j.epsl.2007.06.025.

Reutenauer, C., Landais, A., Blunier, T., Bréant, C., Kageyama, M., Woillez, M.-N., Risi, C., Mariotti, V., Braconnot, P., 2015. Quantifying molecular oxygen isotope variations during a Heinrich stadial. Clim. Past 11, 1527–1551. https://doi.org/10.5194/cp-11-1527-2015.

Schwander, J., 1989. The transformation of snow to ice and the occlusion of gases. In: Oeschger, H., Langway Jr., C.C. (Eds.), The Environmental Record in Glaciers and Ice Sheets. John Wiley, New York, pp. 53–67.

Seltzer, A.M., Buizert, C., Baggenstos, D., Brook, E.J., Ahn, J., Yang, J.-W., Severinghaus, J.P., 2017. Does δ^{18}O of O_2 record meridional shifts in tropical rainfall? Clim. Past 13, 1323–1338. https://doi.org/10.5194/cp-13-1323-2017.

Severinghaus, J.P., Sowers, T., Brook, E.J., Alley, R.B., Bender, M.L., 1998. Timing of abrupt climate change at the end of the Younger Dryas interval from thermally fractionated gases in polar ice. Nature 391, 141–146.

Severinghaus, J.P., Grachev, A., Luz, B., Caillon, N., 2003. A method for precise measurement of argon 40/36 and krypton/argon ratios in trapped air in polar ice with applications to past firn thickness and abrupt climate change in Greenland and at Siple Dome, Antarctica. Geochem. Cosmochim. Acta 67, 325–343. https://doi.org/10.1016/S0016-7037(02)00965-1.

Severinghaus, J., Battle, M., 2006. Fractionation of gases in polar ice during bubble close-off: new constraints from firn air Ne, Kr and Xe observations. Earth Planet Sci. Lett. 244, 474–500. https://doi.org/10.1016/j.epsl.2006.01.032.

Severinghaus, J.P., Beaudette, R., Headly, M.A., Taylor, K., Brook, E.J., 2009. Oxygen-18 of O_2 records the impact of abrupt climate change on the terrestrial biosphere. Science 324, 1431–1434. https://doi.org/10.1126/science.1169473.

Shackleton, N.J., 2000. The 100,000-year ice-age cycle identified and found to lag temperature, carbon dioxide, and orbital eccentricity. Science 289, 1897–1902.

Shackleton, N., Fairbanks, R., Chiu, T., Parrenin, F., 2004. Absolute calibration of the Greenland time scale: implications for Antarctic time scales and for Δ14C. Quat. Sci. Rev. 23, 1513–1522. https://doi.org/10.1016/j.quascirev.2004.03.006.

Spahni, R., Chappellaz, J., Stocker, T.F., Loulergue, L., Hausammann, G., Kawamura, K., Flückiger, J., Schwander, J., Raynaud, D., Masson-Delmotte, V., Jouzel, J., 2005. Atmospheric methane and nitrous Oxide of the late pleistocene from Antarctic ice cores. Science 310, 1317–1321. https://doi.org/10.1126/science.1120132.

Stolper, D.A., Bender, M.L., Dreyfus, G.B., Yan, Y., Higgins, J.A., 2016. A Pleistocene ice core record of atmospheric O_2 concentrations. Science 353, 1427–1430. https://doi.org/10.1126/science.aaf5445.

Suwa, M., Bender, M.L., 2008. Chronology of the Vostok ice core constrained by O_2/N_2 ratios of occluded air, and its implication for the Vostok climate records. Quat. Sci. Rev. 27, 1093–1106. https://doi.org/10.1016/j.quascirev.2008.02.017.

Veres, D., Bazin, L., Landais, A., Toyé Mahamadou Kele, H., Lemieux-Dudon, B., Parrenin, F., Martinerie, P., Blayo, E., Blunier, T., Capron, E., Chappellaz, J., Rasmussen, S.O., Severi, M., Svensson, A., Vinther, B., Wolff, E.W., 2013. The Antarctic ice core chronology (AICC2012): an optimized multi-parameter and multi-site dating approach for the last 120 thousand years. Clim. Past 9, 1733–1748. https://doi.org/10.5194/cp-9-1733-2013.

Wang, Y.J., Cheng, H., Edwards, R.L., An, Z.S., Wu, J., Shen, C.-C., Dorale, J.A., 2001. A high-resolution absolute-dated late pleistocene monsoon record from hulu cave, China. Science 294, 2345–2348. https://doi.org/10.1126/science.1064618.

Wang, Y.J., Cheng, H., Edwards, R.L., Kong, X., Shao, X., Chen, S., Wu, J., Jiang, X., Wang, X., An, Z., 2008. Millennial- and orbital-scale changes in the East Asian monsoon over the past 224,000 years. Nature 451, 1090–1093. https://doi.org/10.1038/nature06692.

Yu, Z., Loisel, J., Turetsky, M.R., Cai, S., Zhao, Y., Frolking, S., MacDonald, G.M., Bubier, J.L., 2013. Evidence for elevated emissions from high-latitude wetlands contributing to high atmospheric CH_4 concentration in the early Holocene. Global Biogeochem. Cycles 27, 131–140. https://doi.org/10.1002/gbc.20025.